IV. STARTUP DYNAMICS AND CONTROL*

Herbert J. Heppler, Jr., Benjamin H. Colmery,
James J. Watt, and Vernon D. Gebben

Various components of nuclear rockets are discussed in the paper on PROPELLANT FLOW SYSTEM COMPONENTS and the paper on HEAT TRANSFER AND FLUID MECHANICS. A useful propulsion system requires the integration of these components into a single entity whose operation is harmonious and controllable. Some of the Lewis efforts in system investigations and control development are presented in this paper. Specific attention is given to flow system startup characteristics and two-phase hydrogen flow characteristics. In the controls area, the application of pneumatic components, or fluidic devices, is discussed.

NUCLEAR-ROCKET COLD-FLOW STARTUP

Benjamin H. Colmery

INTRODUCTION

A nuclear-rocket engine in space probably will use no special startup equipment; it will rely on a "bootstrap" technique starting procedure. Run-tank pressure drives hydrogen propellents through the flow system. The liquid hydrogen acquires heat from the engine components, and a portion of the heated hydrogen is bled to the turbine. This bleed gas powers the turbine, which in turn accelerates the pump increasing the flow and pressure through the system. Successful bootstrap results in a continuous increase of system flow and pressure.

The bootstrap technique has been used successfully to start chemical-rocket engines, but there are significant differences in the nuclear-engine bootstrap. One difference is the much longer time for the nuclear rocket to be brought to power. Also, all the propellant is utilized, and it follows a more complex hydrogen flow path in the nuclear rocket. These factors coupled with the lack of precise knowledge of two-phase hydrogen flow and boiling phenomena caused concern as to whether unacceptable flow perturbations might

occur during bootstrap startup. Further, there was uncertainty as to whether enough energy could be delivered to the turbine at low pump speeds to cause flow acceleration. Also, there was the usual question of unanticipated problems in new hardware.

Therefore, a full-scale test of the bootstrap startup of a nuclear-rocket engine was undertaken - the first such test ever made. The Nuclear-Rocket Cold-Flow Test Facility used (fig. IV-1) is located at the Plum Brook Station of the Lewis Research Center. The altitude exhaust system shown enabled maintaining a rocket-nozzle-exhaust pressure of nominally 0.5 pound per square inch absolute throughout each run. The rocket engine was mounted in the 130-foot-tall structure at the right in a down-firing position.

SYMBOLS

A	cross-sectional flow area, ft^2
A_{ht}	heat-transfer area, ft^2
C_p	specific heat of wall material, $Btu/(lb)(^oR)$
d	diameter of flow passage, ft
g	acceleration of gravity, ft/sec^2
H	heat-transfer coefficient, $Btu/(ft^2)(^oR)(sec)$
h	fluid enthalpy, Btu/lb
I	turbopump moment of inertia, (ft-lb)(sec)/rpm
K	loss coefficient
K_n	choked-nozzle flow coefficient, $(ft^2)(^oR)^{1/2}/sec$
k	fluid thermal conductivity, $Btu/(ft)(^oR)(sec)$
L_p	pump torque, ft-lb
L_t	turbine torque, ft-lb
M	mass of wall material, lb
N	turbopump speed, rpm
P	fluid pressure, lb/ft^2
ΔP	component pressure drop, lb/ft^2
Pr	fluid Prandtl number
P_{nc}	nozzle chamber pressure, lb/ft^2
ΔP_p	pump pressure rise, lb/ft^2

P_{ti}	turbine-inlet fluid pressure, lb/ft^2
P_{to}	turbine-outlet fluid pressure, lb/ft^2
Q	heat addition from surroundings, Btu
R	gas constant, $ft/^oR$
Re	fluid Reynolds number
T	fluid bulk temperature, ^oR
T_{nc}	nozzle chamber temperature, ^oR
T_s	saturated-fluid bulk temperature, ^oR
T_{ti}	turbine-inlet fluid bulk temperature, ^oR
T_w	wall temperature, ^oR
t	time, sec
V	volume of lump, ft^3
W	weight flow, lb/sec
ΔW	empirical weight flow storage, lb/ft^2
W_n	nozzle flow, lb/sec
W_p	pump weight flow, lb/sec
W_t	turbine weight flow, lb/sec
ΔX	length of lump, ft
ρ	fluid density, lb/ft^3

SYSTEM DESCRIPTION

A schematic diagram of the rocket-engine test package is shown in figure IV-2, and a photograph of some of the hardware is shown in figure IV-3. The test hardware consisted of a turbopump assembly, unfueled reactor, and a supersonic exhaust nozzle. The liquid-hydrogen run tank, which feeds the pump, has a capacity of 2000 gallons and has a servo-controlled pressurizing system. An 8-inch-diameter line, which is equipped with a turbine-type flowmeter, connects the pump to the run tank.

The turbopump assembly consisted of a Rocketdyne MARK-IX turbopump, turbine-power-control valve, and turbine bleed line. The liquid-hydrogen pump is composed of an axial-entrance mixed-flow axial-discharge inducer stage, six identical high-pressure axial-flow stages, and a single-outlet collecting volute. The pump is designed for opera-

tion with liquid hydrogen and is capable of providing the flow rate and pressure requirements of a NERVA type engine.

The turbine is a six-stage pressure-compounded axial-flow unit designed for operation with hot or ambient temperature gaseous hydrogen. The unit was designed to deliver 15 000 horsepower and is capable of deliverying NERVA power requirements with ambient temperature hydrogen.

The pump discharges into a 4-inch-diameter stainless-steel flight-weight feed line equipped with a servocontrolled butterfly valve used for flow control. Approximately 18 feet downstream from the main flow-control valve, the propellant line is divided equally into three $2\frac{3}{8}$-inch-diameter ducts that feed the nozzle inlet manifold.

The regeneratively cooled (liquid hydrogen) tubular-wall nozzle utilizes single-pass cooling. The liquid hydrogen enters the tubes through three equally spaced inlet connections on the manifold and flows toward the reactor end.

On discharging from the nozzle coolant tubes, the fluid enters the reflector inlet manifold section of the reactor assembly. From there it passes through the reflector component that is composed of the inner graphite reflector, an outer aluminum reflector, simulated aluminum control rods, and the aluminum pressure vessel. The fluid then enters the reactor core; flowing through the many parallel coolant passages in the unloaded graphite reactor core.

The warm hydrogen emerges from the core into the regeneratively cooled nozzle thrust chamber where most of it is exhausted into the facility vacuum exhaust (0.5 psia). A small portion of the fluid, however, is bled by a 3-inch-diameter bleed port, turbine-gas bleed line, and servocontrolled turbine-power-control valve, to the turbine. Altogether, the rocket-engine system tested was a full-scale model of what might have been a flight version of a system using the Kiwi B-1 reactor.

One objective of this startup program was to determine the bootstrap capability of the nuclear-rocket engine for a range of tank pressures and the influence of two-phase flow and pump stall on the startup. A second objective was to develop an analytical technique that would dynamically simulate the startup and be useful as a general tool to predict startup characteristics.

EXPERIMENT PROCEDURES

Two kinds of experimental runs were undertaken: cooldown and bootstrap. The cooldown tests were undertaken to examine the problems of boiling and two-phase flow. In these runs, the pump was chilled to liquid-hydrogen temperatures. Then, at zero run time, the pump-discharge valve (fig. IV-2) was opened, and run-tank pressure forced flow through the system to the facility vacuum exhaust. The run was continued until the

engine components had cooled and flow had stabilized. Unlike later bootstrap tests, the turbine-power control valve was kept closed throughout the cooldown run. Hence, it was possible to examine the two-phase flow and boiling instabilities without the additional complications of turbopump-load interactions and the dynamics associated with a rapid increase in flow and pressure. Ten cooldown runs were made with run tank pressures of 25, 35, and 50 pounds per square inch absolute.

In the bootstrap runs, the pump was chilled to liquid-hydrogen temperatures, and at zero time, the pump-discharge valve was opened and flow was established in the system. The turbine-power-control valve was opened at run times varying from 0 to 10 seconds and was controlled by various schemes to maintain desired pump acceleration. The run was continued, generally, until peak values of pump speed, weight flow, and pump pressure rise had been achieved. To date, 15 bootstrap runs have been made.

RESULTS AND DISCUSSIONS

Cooldown Tests

Three cooldown tests corresponding to run-tank pressures of 25, 35, and 50 pounds per square inch absolute are shown in figure IV-4. The time history of the static pressure at the nozzle coolant inlet shows two types of oscillations. There is an initial transient with a nominal disturbance frequency of about 2 cps, which is called initial surge. A second mode of oscillation, called two-phase-flow perturbations, follows with an initial frequency of about 15 cps.

The initial surge was an expected phenomenon. Undoubtedly, it is the result of the introduction of liquid hydrogen at cryogenic temperature into a pipe at ambient room temperature. When the hydrogen flashes into vapor it produces the pressure surge. The phenomenon occurred as soon as the pump-discharge valve was opened, and it died away in about 2 seconds. It originated in the lower part of the pump-discharge line as a pressure disturbance; this disturbance proceeded upstream and downstream from the point of origin and was closely followed by corresponding changes in hydrogen weight flow and fluid temperature. The initial surge, which occurred on both the cooldown and the bootstrap runs, died away with an oscillation frequency of about 2 cps. The initial surge was the largest flow-system perturbation encountered.

Normalized peak surge amplitude is plotted against run-tank pressure in figure IV-5. The initial peak pressure is sensitive to run-tank pressure with the higher tank pressures attenuating the pressure surge. Also shown in the figure is an unexpected effect - an apparent dependence on the weight of the pump-discharge-line flanges and gimbals, as indicated by the two curves.

The flanges and gimbals on the pump-discharge line were changed after the first 12 test runs. Boiler-plate-weight flanges (about 31 lb each) were replaced by flight-weight flanges (about 3 lb each), and lighter gimbals were used. The replacement hardware was made of the same materials as the old. The internal dimensions and finish specifications were unchanged, and the piping was not changed - only the flange and gimbal mass were changed. Prior computations and intuition indicate that the smaller heat capacity of the smaller mass should have negligible effect on heat transfer in the pump-discharge line during the first few seconds of hydrogen flow; hence, it was anticipated that the change in mass would not affect the amplitude of the initial surge.

A possible explanation of the existence of two curves in figure IV-5 is the effect of vibration on the heat-transfer coefficient for fluid flow in a pipe. Literature exists on the interaction between vibration and heat transfer which indicates that lateral oscillations of a pipe containing flowing hydrogen substantially augment the heat-transfer process under some conditions (ref. 1, p. 133). The pipe with the lighter flanges could vibrate with higher lateral velocities. The largest velocities would result sequentially in more fluid turbulence, larger heat transfer, a larger rate of vaporization of liquid hydrogen, hence, a larger pressure surge.

Because the phenomenon was unexpected, the pump-discharge line had not been instrumented for vibration. Hence, verification of the foregoing hypothesis has not yet been made.

The second kind of disturbance (fig. IV-4), termed two-phase-flow perturbation, commenced about 2 seconds after flow initiation. The two-phase-flow perturbations were found to originate as pressure disturbances, and these pressure disturbances were transmitted upstream and downstream from the point of origin.

The pressure disturbances were accompanied by flow and temperature changes. The flow changes occurred out of phase with the pressure disturbances. Temperature variations of the fluid were observed at a given point until the hydrogen temperature reached saturated liquid temperatures at that point; subsequently, flow and pressure disturbances continued, but temperature oscillations were no longer apparent.

As shown in figure IV-4, the amplitude of oscillations appears unaffected by run-tank pressure, but the duration of the oscillation is shortened with higher tank pressure.

Bootstrap Capability

Results of a typical controlled bootstrap run are shown in figure IV-6. The upper curve shows the pump operating map. The pump stall line is depicted as a band, because of hysteresis effects of entering and leaving stall, and because of uncertainties in the precise location of the stall line at low pump speeds. The lower curve shows pump speed as

a function of time. Points A and B in both figures correspond to the same points in time. This test run is termed controlled because a closed-loop control system was used to maintain a desired rate of pump acceleration.

Events in the run occurred as follows: At zero time, the pump metal had been chilled to liquid-hydrogen temperature and the pump-discharge valve was opened. As flow was initiated, there were sharp pressure surges in the regions downstream of the pump-discharge valve. The surges were followed by rapid pressure oscillations at a frequency of about 15 cps, similar to those obtained in the cooldown runs. These oscillations have been omitted during the first 6 seconds of the run in the upper curve of figure IV-6. The pump initially windmilled to point A because of the liquid hydrogen flowing through it, forced by tank pressure.

At 6 seconds, point A, the turbine-power-control valve was opened and commanded to achieve a pump acceleration of 200 rpm per second. It can be seen in the lower curve of figure IV-6 that this acceleration was quickly achieved and held smoothly. In the upper curve (fig. IV-6) buildup of pump pressure rise and of hydrogen flow occurred. There were pressure and flow disturbances, but they were small. The operating point skirted the stall region, reached an operating peak in flow and speed at about point B, and then faded back to the origin.

The peak at point B occurred because the turbine-inlet fluid energy became insufficient to continue accelerating the turbopump. This fluid energy, acquired from the latent heat energy of the engine components, decreases as the system cools. In an actual flight startup, nuclear power would have become the dominant energy source somewhere between times A and B, and the bootstrap acceleration would have continued to the desired system operating point.

Figure IV-7 shows data from a typical uncontrolled bootstrap test plotted on the pump operating map. This run is called an uncontrolled run because both the pump-discharge valve and the turbine-power-control valve were opened fully at zero run time and kept fully open until the end of the run. This uncontrolled bootstrap gave the fastest increase in pump speed, flow, and pressure, and it also gave the largest flow disturbances. Initially, there were rapid appreciable variations in flow and pressure. The pump windmilled for a few seconds until adequate power arrived at the turbine to cause it to accelerate. Then there was a rapid buildup of pump speed, pressure, and flow.

The initial flow and pressure disturbances were damped during the bootstrap acceleration. The pump entered the stall region. Flow and pressure oscillations were observed that continued until the pump left the stall region. Nevertheless, bootstrap continued, and the pump acceleration was nearly constant at 1150 rpm per second. Maximum values for pump speed, pressure rise, and flow (10 000 rpm, 100 psi, and 30 lb/sec, respectively) were achieved in about 12 seconds; these are appreciable values of the rated Kiwi B-1 operating point.

The tests described by figures IV-6 and IV-7 show that, neglecting weightlessness and the complications introduced by nuclear operations, a bootstrap start could be accomplished. They show that appreciable values of pump speed, liquid-hydrogen flow, and pump pressure rise could be achieved by using latent heat of the engine components (at ambient atmospheric temperatures), and that peak values could be built up in as little as 12 seconds.

In tests not illustrated, it was also shown that bootstrap runs could be successfully accomplished at a run-tank pressure of 25 pounds per square inch absolute. The lower the run-tank pressure, the lower the overall tank weight; hence, insofar as the bootstrap operation is concerned, it appears that lighter weight tanks might be used.

Operational Problems

Several system and equipment operating problems were encountered during the runs, and an interesting one is shown in figure IV-8. The interest arises because of the erroneous appearance that the severe oscillations were simply a result of the system operating point being accelerated into the pump stall region. In fact, the oscillations were the result of gas ingestion.

The axial pump used counteracts axial thrust with a balance piston. A bleed line from the region of the balance piston had been installed to empty upstream of the pump inlet. In posttest analysis, it was found that during cooldown, a check valve prevented the bleed line from being fully chilled to liquid-hydrogen temperature. Hence, when the pump acceleration occurred, the bleed line discharged gas rather than liquid into the pump inlet.

The bleed line was modified to enable complete cooling, and the run of figure IV-8 was repeated under otherwise identical conditions. The result is shown in figure IV-9. It is clear that removal of the bleed-line heat source removed the oscillations. The two figures also illustrate what might happen if gas were entrained in the liquid that leaves the run tank during bootstrap.

Other operational problems encountered were straightforward, correctable ones involving cryogenic temperatures or random equipment malfunctions.

Analytical Simulation

The goal of an analytical effort at Lewis has been to develop a mathematical model to simulate the nuclear-rocket-engine startup. The system was studied by dividing the model into spacial lumps, each representing a specific hardware component of the research

apparatus shown in figure IV-2. These lumps can then be grouped, as in figure IV-10, into a system block diagram composed of a pump, feed line, nozzle coolant tubes, reflector, core, thrust nozzle, turbine bleed line, turbine-power-control valve, and turbine. The lumping was done in this manner to take advantage of system geometry and data probe locations and also to limit the amount of necessary analog computing equipment.

The state of the fluid varies throughout the system during the course of a run. With liquid hydrogen flowing into the system, the material of the components begins to cool by giving up latent heat to the fluid. Throughout every experimental run, it was observed that a definite, but changing, portion of the system contained two-phase fluid. The preceding portion was all liquid, while the remaining portion downstream was all gas, as illustrated in figure IV-11. As the run proceeded and the system cooled, the two-phase section moved downstream.

During the time of simulation, the range of the fluid state was specified for each lump; all liquid in the pump, the possibility of liquid, two phase, or gas between the feed line inlet and the reflector exit, and all gas throughout the balance of the system.

The differential equations describing each lump were written and then programmed on the analog computer. For purposes of presenting the system equations, they can be grouped into those pertaining to the turbopump assembly and those concerning the load.

Turbopump Assembly

As stated earlier, the turbopump is a MARK-IX axial-flow liquid-hydrogen pump and six-stage turbine. This unit is described by the following equations:

$$\Delta P_p = N^2 f_1\left(\frac{W_p}{N}\right) \tag{1}$$

$$L_p = N^2 f_2\left(\frac{W_p}{N}\right) \tag{2}$$

$$\frac{dN}{dt} = \frac{30}{\pi I}\left(L_t - L_p\right) \tag{3}$$

$$L_t = W_t f_3\left(N, T_{ti}, \frac{P_{to}}{P_{ti}}\right) \tag{4}$$

$$W_t = \frac{P_{ti}\left[1 - \left(\frac{P_{to}}{P_{ti}}\right)^2\right]}{T_{ti}} f_4 \frac{N}{\sqrt{T_{ti}}} \tag{5}$$

Equations (1) and (2), the pump-head-rise and torque-characteristic equations, respectively, are empirically derived from the manufacturer's rated speed operating data and from experimental low-speed data. The balance of the equations was generated from a more theoretical basis, namely, from torque and momentum considerations.

As stated earlier, the turbine is powered by a controlled flow of gas that is fed through the turbine bleed line from the nozzle thrust chamber. The representation for this bleed line is adequately described by the all-gas-lump equations presented in the following section.

Load

The load segment of the model was broken into five major spacial lumps: feed line, nozzle coolant tubes, reflector, core, and thrust nozzle. In general, the equations for each lump are as follows: the conservation of fluid mass, the conservation of fluid momentum, the conservation of fluid energy, the conservation of thermal energy of the material parts, Newton's law of cooling, and the fluid state properties. The written forms of these equations are, respectively,

$$\frac{dR}{dt} = \frac{1}{V}\left(W_{in} - W_{out}\right) \tag{6}$$

$$\frac{dW}{dt} = \frac{gA}{\Delta X}\left(P_{in} - P_{out}\right) - \frac{K}{2V}\frac{W^2}{\rho} - \frac{1}{V}\left(\frac{W_{out}^2}{\rho_{out}} - \frac{W_{in}^2}{\rho_{in}}\right) \tag{7}$$

$$\frac{dh}{dt} = \frac{1}{\rho V}\left[\frac{dQ}{dt} - W\left(h_{out} - h_{in}\right)\right] \tag{8}$$

$$\frac{dT_w}{dt} = -\left(MC_p\right)^{-1}\frac{dQ}{dt} \tag{9}$$

$$\frac{dQ}{dt} = HA_{ht}\left(T_w - T\right) \tag{10}$$

$$P = f_5(\rho, h) \tag{11}$$

$$T = f_6(p, h) \tag{12}$$

For an all-gas lump, the general equations (6) to (12) apply directly with the following qualifications: First, the fluid temperature (eq. (12)) was assumed to be a function only of the fluid enthalpy. Second, the pressure relation (eq. (11)) was modified into the more conventional gas law:

$$P = R\rho T \tag{13}$$

And finally, the heat-transfer coefficient used in equation (10) was

$$H = 0.021\frac{k}{d}Pr^{0.33}Re^{0.8}\left(\frac{T}{T_w}\right)^{0.575} \tag{14}$$

For an all-liquid lump, the general equations (6) to (12) also apply directly, if the appropriate heat-transfer coefficient is assumed. In addition, the fluid-temperature state equation (eq. (12)) can be simplified if saturated liquid hydrogen is assumed:

$$T = f_7(P) = T_s \tag{15}$$

Theoretically, the general equations (6) to (12) could be used for a two-phase lump if homogeneous flow and thermodynamic equilibrium between the phases are assumed. A pressure state relation (eq. (11)) has been derived from existing two-phase-properties tables, and the fluid-temperature state would be that of saturated liquid hydrogen (eq. (15)). Because of the complexities and uncertainties in arriving at a two-phase pressure loss coefficient K and a two-phase heat-transfer coefficient H, experimental data were used to modify empirically the momentum equation (eq. (7)) and the heat-transfer equation (eq. (10)). In the case of the heat-transfer relation, a correlation of the form in figure IV-12 was derived from experimental data and found to be an adequate representation for the overall average heat transfer in a two-phase lump.

However, in an analog simulation employing these two-phase equations, the fluid-pressure relation (eq. (11)) proved to be too cumbersome for practical use. Therefore, a more convenient form of the state relation, one relating the two-phase density to the

pressure and enthalpy (eq. (16)), was used. Unfortunately, the utilization of this equation necessitated alternate forms for the conservation equations of mass and momentum (eqs. (6) and (7)) The modified equations are as follows:

$$\rho = f_8(h, P) \tag{16}$$

$$W_{out} = W_{in} - \Delta W \tag{17}$$

$$\Delta P = \frac{\Delta X}{gA}\left[\frac{K}{2V}\frac{W^2}{\rho} + \frac{1}{V}\left(\frac{W_{out}^2}{\rho_{out}} - \frac{W_{in}^2}{\rho_{in}}\right)\right] \tag{18}$$

Note the missing derivatives of density and weight flow in equations (17) and (18), respectively. The lack of a convenient expression relating pressure to a function of density and enthalpy forced dropping these derivatives. In turn, the flow dynamics that are characteristic of the two-phase lump were thus removed. Detailed investigation has shown that this two-phase dynamic response is a necessary factor in determining low-frequency system dynamics. Hence, the model as presented herein must be considered a quasi-steady-state simulation.

Thus, the system load consists of a thrust nozzle plus four lumps, modeled after the gas described previously, liquid, or two-phase representations. Within a fraction of a second after flow initiation, the gas side of the nuclear-rocket nozzle may be considered choked at the throat. The choked, isentropic nozzle weight flow is given by

$$W_n = K_n \frac{P_{nc}}{\sqrt{T_{nc}}} \tag{19}$$

Simulation of the previously discussed controlled and uncontrolled bootstrap tests are presented in figures IV-13 to IV-16. In the first case, the pump speed was controlled in such a manner that the pump stall was avoided, while in the second case, the system was accelerated in an uncontrolled manner with no attempt made to avoid the stall region.

For the controlled bootstrap tests, after a 6-second period of pump windmilling, the turbine-power-control valve was opened and bootstrapping commenced. There were initial flow oscillations but they were damped out as bootstrapping proceeded. The system operating point steadily increased to a maximum pump pressure rise.

The simulation was initiated 5 seconds after the start of the experimental run because of the range limitations of the analog computer. Most of the initial oscillations had died out by 5 seconds; those remaining, however, could not be duplicated by the model because

of the missing two-phase dynamic terms. The steady-state level approximated the pump map data (fig. IV-13) and the parameter-time data (fig. IV-14); the simulated pump correctly operated out of the stall region during the entire computer run.

The second run was an uncontrolled bootstrap test. It was uncontrolled because the turbine-power-control valve was opened fully at the beginning of the test and kept fully open until the end. The initial flow oscillations were once again damped out as bootstrapping commenced. Stall-induced flow oscillations were observed during a portion of the run as the system bootstrapped through stall to a maximum pump pressure rise and weight flow.

The simulation of the second test began 3 seconds after the actual experimental system startup. The simulated pump entered and operated in the stall region, but the analytical model was unable to produce the stall-induced flow oscillations, as indicated in figure IV-15. The parameter-time data is presented in figure IV-16.

For both tests, the model matched the experimental data for most parameters to within 10 to 25 percent of the measured quantities. The only exceptions to this are the turbine weight flow and certain other parameters that disagreed in the initial low level portions of the runs.

CONCLUSIONS

The conclusions drawn from the experimental bootstrap startup operations conducted to date have the qualifications that nuclear operations and weightlessness were not included, and that there are a number of boiling and two-phase-flow phenomena that still are not explained. With these qualifications, it can be stated that

1. The bootstrap operation was performed successfully. Appreciable percentages of the rated operating conditions of system flow rate, pressures, and pump speed were achieved.

2. Bootstrap was accomplished successfully at a run-tank pressure of 25 pounds per square inch absolute; this may have important implications on run-tank weight.

3. Flow disturbances encountered would not cause concern about the practicability of a nuclear bootstrap startup on a flight mission.

A quasi-steady-state model has been developed to simulate a nuclear-rocket cold-flow system. In general, the experimental data were matched to within 10 to 25 percent of the measured values. The effort demonstrated that a complex system, such as a nuclear-rocket engine, may be simulated with a fairly simple model. It has demonstrated the necessity for including two-phase flow dynamics. The quasi-steady-state model paves the way for more detailed studies in the areas of two-phase flow dynamics, heat transfer, and friction pressure drop.

ANALYSIS OF HYDROGEN FLOW CHARACTERISTICS AT SUBCRITICAL PRESSURES

James J. Watt

INTRODUCTION

Some highlights from a program conducted at Lewis to provide support for the development of the nuclear rocket in the area of component heat-transfer and flow analysis are described. Only two phases of the reactor operating spectrum were considered, the startup and after-cooling phases, both of which involve hydrogen at subcritical pressure.

TRANSIENT ANALYSIS

For startup analysis, the two-phase and gas flow regions were considered. Correlations for local heat transfer and pressure drop were included in a transient-analysis procedure. The purpose of the procedure is to predict as a function of time in a given engine component the following conditions: fluid pressure and temperature profiles along the length, depth of two-phase penetration, wall temperature profiles both axially and longitudinally, and flow distribution when parallel passage components were considered. Input to this transient procedure included the geometry and material properties of the component and the initial distribution of material temperatures. Input provided as a function of time during the transient were the flow rate, inlet fluid pressure, and inlet enthalpy. A quasi-steady-state approach was used in flow analysis, that is, flow and heat-transfer conditions were defined periodically during the transient, and the changes in material temperature were calculated on the interval between flow calculations.

Chilldown experiments were performed on single and multiple channel test sections that simulated conditions in the reactor components during the startup transient. Liquid hydrogen flowing from a pressurized supply tank was introduced into test sections initially at room temperature. Flow continued until the test section was chilled to near liquid hydrogen temperature. Figures IV-17 to IV-19 are photographs of three test sections used in chilldown experiments. A single tube 55 inches long with a 0.75-inch outside diameter and a 0.188-inch inside diameter is shown in figure IV-17. A five-passage test section is shown in figure IV-18, and a 33-passage test section representing 1/24 of a nuclear-rocket reflector annulus is shown in figure IV-19. Tests were performed in an evacuated enclosure to reduce the convective heat transfer from the outer surfaces of the test sections.

The experimental flow rate and test-section-inlet conditions along with the initial

material temperature distribution were then used as input to the transient-analysis procedure. The usefulness of this procedure was then evaluated by comparison of predicted and experimental results.

The results of some of the earlier experiments are included in reference 2 (p. 133). The results of applying the transient-analysis procedure to the reflector during the full-scale nuclear-rocket bootstrap startup tests performed at the Lewis Plum Brook Station are presented in paper III. A more complete description of the transient-analysis procedure and a comparison of its predictions with experimental results obtained from chilldown experiments on a single tube (fig. IV-17) are the subject of a current investigation (unpublished data obtained by F. C. Chenowith, J. J. Watt, and E. L. Sprague of Lewis).

A comparison of single-tube chilldown experimental results with predictions illustrates the current status of transient analysis. The measured wall temperatures along the length of the test section are indicated at 3.0, 8.0, and 13.0 seconds during a chilldown run in figure IV-20. The solid lines are the predicted temperature profiles. Before zero time, the test section had a nearly constant wall temperature of 522° R. At zero time, liquid-hydrogen flow was started into the test section. The thin-walled 3-inch-long dip tube at the inlet chilled rapidly. Because there was no temperature instrumentation until the 7-inch station, the accuracy of prediction in this region cannot be evaluated. There is a dip in the predicted wall-temperature profile that occurs at the point of transition from two phase to all gas in the flow passage. The length at which this transition occurred is indicated by the dashed veritical lines for each time. The tip or disparity in predicted wall temperature increases in both amplitude and length with time. Further into the all-gas region, it may be noted that good agreement between predicted and experimental wall temperatures was obtained.

The reason for the dip in predicted wall temperatures is indicated in figure IV-21, where the heat-transfer coefficients predicted by the two-phase and gas correlations 11.0 seconds after the start of a chilldown run are plotted. Heat is being transferred from the wall to a two-phase fluid for the first 13 inches and to a gas for the remainder of the passage. As shown in figures IV-20 and IV-21, the peak heat-transfer coefficient occurring near the end of the two-phase region causes the dip in predicted wall temperatures, and the decrease in heat-transfer coefficient at the transition to gas (38 percent, in this case) causes the sharp increase in wall temperature. The minimum of the dip lags the two-phase to gas transition point because of time history effects as the two phase penetrates progressively further into the passage during the chilldown

These disparities occur in a region that requires a research effort. The two-phase correlation used (ref. 3, p. 133) was based on an experimental effort that considered qualities less than 0.8. The gas correlation (ref. 4, p. 133) was based on experiments performed with bulk temperature far removed from saturation temperatures. The disparity, therefore, occurs at the intersection of two extrapolated correlations.

Heated-tube experiments performed with hydrogen gas at temperatures near saturation temperature (unpublished data obtained by H. J. Gladden and J. J. Watt of Lewis) have indicated that there is a bulk temperature effect on gas heat transfer. These experiments also indicated a strong increase in heat-transfer coefficient near the entrance of a passage when velocity and temperature profiles develop concurrently.

In summary, the transient-analysis procedure is a useful tool for predicting the general characteristics of flow and heat transfer in passages that contain boiling hydrogen. There are local limitations because conditions occur where current correlations for heat transfer are not directly applicable. These limitations become significant if thermal-stress calculations are to be performed, based on predicted material temperature profiles.

PARAMETRIC STUDY

A system model developed for the cold-flow startup of the nuclear rocket was discussed in the previous section. This model includes the characteristics of the pump, turbine, nozzle, control valves, and reactor. Its weakness was in the areas related to two-phase hydrogen. For purposes of heat-transfer and flow calculations in the model, a series of single passages was used to simulate the flow system. In order to include the two-phase hydrogen heat-transfer and flow characteristics in the model, it was necessary to test the system to gain empirical characteristics. The usefulness of this approach is thus limited because system analysis cannot be performed until the system of interest is built and tested.

A parametric study was made which demonstrates that the overall characteristics of each of the components in a given system could be analytically predicted and that these characteristics could be expressed as functions of fundamental variables over the range of interest. The flow-calculation portion of the transient-analysis procedure (discussed in the TRANSIENT ANALYSIS section) was utilized for the parametric study. The flow calculation procedure evaluates instantaneous steady-state conditions. Continuity is satisfied, but this procedure does not contain the terms required for a dynamic analysis. The parametric study was also performed to provide more insight into the general characteristics of a system containing boiling two-phase hydrogen.

Basically, three parameters change with time during a bootstrap startup: flow rate, wall temperature, and depth of two-phase penetration. The change in depth of two-phase penetration can be considered for a given component as a change in inlet quality. A single-flow passage representing the reflector is illustrated at the top of figure IV-22.

The influence of the three parameters (inlet quality, flow rate, and wall temperature) on the heat transferred to the fluid passing through the channel is shown by the three curves for the range of interest in startup (fig. IV-22). It may be seen that the overall heat transferred to the fluid Q increases almost linearly with increase in flow rate per

unit flow area G, and also with increase in wall temperature. As the heat transfer Q is nearly independent of changes in inlet quality, figure IV-22 suggests that Q in a portion of the system containing two-phase hydrogen might be expressed as a function only of G and wall temperature.

Correlations for overall heat transfer for the reflector and for the pump-discharge line are shown in figure IV-23 as functions of G and $T_{wall} - T_{liquid}$. Points for the reflector were generated by performing a series of steady-state calculations over the range of conditions expected during startup; wall temperatures from 100° to 500° R, inlet qualities of 0 and 0.4, and three flow rates. The points form a straight line and the equation for the line is

$$Q = 0.00123\, G^{0.8}(\Delta T - 30)$$

where $\Delta T = T_{wall} - T_{liquid}$ and T_{liquid} is the saturation temperature for the inlet pressure. The reflector is an efficient heat exchanger in the sense that the passages are long and the ratio of heat-transfer surface area to flow area is large. Even with saturated liquid entering the passage, boiling occurred quickly under most conditions, and the predominate heat-transfer mode was from the wall to a gas.

The correlation for the pump-discharge line took the form

$$Q = 0.82 \times 10^{-4}\, G^{0.8}(\Delta T)^2$$

This line, 20-feet long and 4.3 inches in diameter, had comparatively little heat-transfer surface area. For the range of conditions considered during startup, the two phase penetrated the entire length. The difference between the correlations for the reflector and pump-discharge line is a result primarily of the fact that the heat transfer was predominately to a gas in the reflector and predominately to two phase in the pump-discharge line. The form of the equation for the discharge line is somewhat surprising, but it merely reflects the characteristics of the local two-phase correlation (ref. 3, p. 133) as applied to the given geometry and conditions to obtain an overall correlation.

The pump-discharge line of the full-scale nuclear-rocket system at Plum Brook was instrumented for heat-transfer studies. The solid points near the curve for the pump-discharge line are experimental values obtained during bootstrap tests. The agreement with the open symbols (calculated points) is most encouraging.

The foregoing discussion indicates that if the single-passage-simulation geometry and range of expected conditions for a component are known, the current prediction techniques are adequate to be used in developing overall heat-transfer correlations for each lump of a system. It also illustrates that the correlations can be expressed as a function of G and ΔT. Correlations for the pressure drop in a lump or portion of the system were

found to be more complex functions of the three parameters.

The influence on the pressure profile in a typical reflector passage of changes in inlet quality is shown in figure IV-24. The depth of two-phase penetration is indicated by a film-boiling model in the upper figures for three inlet qualities X_{inlet} of 0, 0.35, and 0.5. It may be noted that the lower the inlet quality, the greater the depth of penetration into the passage.

The calculated pressures along the length for each of the inlet quality conditions are shown in the lower portion of figure IV-24. The perhaps subtle but significant point of this figure is that there is little change in pressure in the two-phase region but a significant change in the all-gas region. Although there is a change in velocity as the hydrogen evaporates, the forces are really quite small and the resulting pressure gradient is small compared with the pressure drop occurring in the gas region where the fluid temperature and viscosity increase as the pressure decreases. In order to define the pressure profile in a component or a system, it is essential that the end of the two-phase region be well defined. Not because of forces associated with boiling but rather that the significant pressure changes occur in the all-gas region.

The influence of each of the parameters on the pressure drop in a passage is shown in figure IV-25. All three parameters are shown to exert a strong influence on the pressure drop as they are each varied over their expected range during startup. Whether a quality of 1.0 or 0 is assumed entering the passage makes a difference of two to one in the calculated pressure drop for the conditions of a constant wall temperature and flow rate.

Pressure drop is extremely sensitive to flow rate, as indicated in figure IV-25. Flow rate is an especially difficult parameter to handle accurately during system analysis because of the storage of fluid at various points in the system. The nuclear-rocket system at Plum Brook contained over 30 cubic feet of volume. With the system initially at 0.5 pound per square inch absolute, a significant amount of hydrogen is required to fill the system during a bootstrap startup. For the first 5 to 10 seconds, the flow into the system from the tank far exceeded the outflow from the nozzle throat, and it was 10 to 15 seconds before the outflow started to match the inflow (unpublished data obtained by D. M. Straight, J. J. Biesiadny, J. G. Pierce, and G. W. Metger of Lewis). The time period of this storage effect is dependent on the acceleration rate of the turbopump.

The wall temperature is also shown to have a strong influence on pressure drop. This emphasizes the need, in system analysis, to remove the heat from the system components accurately if valid simulation of pressure drop or pump load is desired.

The combined influence of inlet quality and flow rate is illustrated in figure IV-26 for the typical reflector passage. At low flow rates, there is little influence of inlet quality on the pressure drop. At higher flow rates, inlet quality becomes a sensitive parameter. The family of curves in figure IV-26 is for a wall temperature of 400° R. If a higher wall temperature is assumed, the slope of all the constant flow rates will increase.

For system pressure-drop analysis, computed families of curves relating the three parameters to pressure drop could be provided for each component or lump in the system.

PARALLEL CHANNEL PROBLEM

Figure IV-26 brings out another problem in the analysis of two-phase flow. When flow in parallel passages is analyzed, it is assumed that the total flow will be distributed among the passages in such a way that each passage will have the same overall pressure drop. This flow distribution will be a function of the geometry and surface temperature in each of the passages. Figure IV-26 shows one passage and one wall temperature, but for a given pressure drop, for example, a ΔP of 25 pounds per square inch, there are any number of possible flow rates that could occur depending on the inlet quality.

The problem may be clarified by the example in figure IV-27. Two parallel passages are utilized to simulate the reflector. First, two phase leaves the nozzle coolant passage (sketch at the right of the figure) and is separated by turning into the reflector passages at P_1. Liquid could enter the right passage and gas the left.

A curve for pressure drop as a function of total flow for the separated case is shown at the left. This curve was developed by assuming that the two passages had the same surface temperature and geometry. This assumption permitted obtaining points from figure IV-26. For an assumed pressure drop, flow rates for saturated liquid entering and saturated gas entering were obtained. Summing these two flow rates provides a total flow rate for the assumed pressure drop and therefore a point on the curve. By repeating this process over a range of pressure, the solid line representing the separated case in figure IV-27 was generated.

The curve for the mixed case was obtained as follows: From the points used to generate the separated flow curve, an energy balance was solved to obtain a mixed mean inlet quality. A pressure drop was then obtained which satisfied that inlet quality and total flow rate. By repeating this process several times, the curve for the mixed or homogeneous case was defined.

As shown in figure IV-27, the mixed case always results in a higher calculated pressure drop that could be considered as a maximum. The unmixed case is not a minimum because, if subcooled liquid and superheated gas were assumed, an even lower pressure drop for a given total flow rate would result. The uncertainty in inlet conditions is an unresolved problem in the analysis of two-phase flow in parallel passages. No measurements of either flow or inlet quality are available for the individual passages. The tendency for separation of phases has been observed in multipassage component tests. Much higher pressure drops than recorded experimentally have frequently been calculated. This is traced in part to the assumption in the analysis procedures of perfect mixing.

To our knowledge, there have been no thermal-stress-induced failures in either the

nozzle coolant passages or the reflector due to this separation of phases. Despite this success, if it is desired that reasonable heat-transfer and flow analysis be performed, it is desirable that future inlet plenum designs give as uniform a quality distribution as possible.

The results of this parametric study are summarized by the following points:

(1) Correlations for the overall heat transfer and for the overall pressure drop may be expressed in terms of fundamental variables for each lump of the system when the lump is simulated by a single passage. The overall heat transfer may be expressed as a function of G and ΔT, and the overall pressure drop as a function of X_{inlet}, G, and ΔT.

(2) For a flow passage containing a region of two-phase hydrogen and a region of gaseous hydrogen, pressure drop in the two-phase region is small, but pressure drop in the all-gas region is significant.

(3) For flow through parallel passages, separation of two-phase flow into liquid and gas at the inlets to the parallel passages leads to difficult problems in the analysis of pressure drop, flow distribution, and material temperature profiles.

FLOW AND PRESSURE OSCILLATIONS

"Initial surge" and "two-phase oscillations" were identified during the system tests at Plum Brook and were previously discussed in this paper. Various modes of oscillations were observed during chilldown and heated-tube experiments performed at Lewis. In the paragraphs that follow, four modes of oscillation observed during these component tests are described. This information is presented as a matter of general interest and represents our current interpretation of observed phenomena. Cataloging the modes is hazardous at best because each mode is intimately related to the characteristics of the system in which it occurs. A combination of visual observations and the interpretation of continuous recordings of pressure, temperature, and flow rate were utilized in arriving at these classifications.

Nucleation Source

This mode of oscillation was observed during heated-tube experiments. The model is shown in figure IV-28(a). A glass section just before the heated section permitted the observation of gas bubbles periodically approaching the heated length. The frequency of the appearance of bubbles corresponded to the frequency of measured pressure oscillations.

Gas bubbles entering the boiling section increase the inlet quality. This in turn increases the pressure drop through the boiling section as indicated in figure IV-25. The increase in pressure drop in the boiling section causes a pressure rise at the inlet. This decreases the rate of gas generation from the nucleation source. Thus, a periodic varia-

tion in inlet quality results in oscillations in flow and pressure. A nucleation source resulting from a heat leak to the flow line is used as an example here. Periodic gas generation (flashing) at a restriction before the boiling section can have the same effect. This type of oscillation is seldom severe and can be removed by increasing subcooling of the fluid approaching the boiling section.

Oscillation Source

What is called an oscillation source is indicated as a chamber with a heat source off the main flow line in figure IV-28(b). It frequently appears in the liquid portion of hydrogen flow systems. A real example might be the dead ended leg of a tee in the flow line, or on a smaller scale, a pressure-transducer line. The chamber literally breathes in liquid and breathes out gas. When liquid is breathed in, the flow to the boiling section is reduced; when gas is breathed out, the flow rate and quality approaching the boiling section are altered. The result is periodic flow and pressure oscillations. The amplitude is related to the ratio of the flow in and out of the oscillation source to the through flow in the line. The frequency decreases as the heat flow to the oscillation source is decreased. This type of oscillation may be removed by providing a bleed port on the chamber to remove the gas.

Density Waves

This type of oscillation was observed during heated-tube tests. It would occur when two-phase hydrogen penetrated the entire boiling length. As indicated in the model (fig. IV-28(c)) two-phase hydrogen tends to form a slug-mist-type flow model. When these slugs pass through a restriction, the flow characteristics change, and oscillations in pressure in the boiling section occur. This type of oscillation was observed and the term "density wave" was coined during work reported in reference 5 (p. 133).

Initial Surge

The initial surge oscillations observed during component tests were perhaps less complex than those observed during bootstrap tests because the system was cleaner and interfaces were more clearly defined. The basic description of an initial surge may be made with the aid of the model in figure IV-28(d). The basic elements of the flow system are a precooled length of line, a heated or boiling section, and a restriction in the gas region. For simplicity in this discussion, the liquid-penetration depths at uniform intervals of time are shown by dashed lines labeled alphabetically.

At zero time (point A) pressurized liquid is released into a low-pressure system. Initially, in an attempt to fill the system, the liquid will penetrate too far into the boiling section for stable conditions (point B). At this point gas is being generated faster than it can be removed from the system through the line and orifice at the existing pressure. The velocity (kinetic energy) of the liquid column is dissipated in pressurizing the gas. At point C the liquid velocity is zero and maximum pressure is reached. Because the pressure is greater than the supply pressure, the flow reverses to point D. The combination of effects, caused by the reversed liquid flow and the gas outflow through the restriction reduces the pressure in the boiling section significantly below the supply pressure. The liquid again penetrates deeply into the boiling section, and the cycle is started again. Peak pressures 70 percent greater than supply pressure were observed in the boiling section during chilldown tests of a 1/24 reflector annulus shown in figure IV-19.

The flow system for those chilldown tests is shown schematically in figure IV-29. The test procedure was to pressurize the tank and prechill the flow line to a point just ahead of the reflector inlet plenum. When the line was thoroughly chilled to liquid-hydrogen temperature, flow was directed into the reflector inlet plenum starting the chilldown experiment.

With the aid of high-speed motion pictures, it was observed that the fluid would enter the inlet plenum periodically. This periodic penetration of the liquid into the plenum was related to pressure oscillations in the reflector. When the reflector pressure approached its minimum value, liquid flowed into the plenum. The liquid boiled, and the pressure then increased to values significantly higher than the tank pressure. This high pressure forced the liquid back into the supply line. Boiling stopped and the pressure decreased, thereby completing one cycle.

This oscillation results from an interaction of the inertia of the liquid column, the compressibility of the gas, the boiling process, and the pressure-flow characteristics of the exit orifice. The oscillation is started by the initial flow surge, and it is sustained by periodic boiling.

The influence of the exit orifice size was investigated and is also shown in figure IV-29. The smallest orifice caused the highest pressure peak and this occurred at the lowest frequency. For the largest orifice, the pressure peak was negligible. This example is a fairly simple illustration of the initial surge phenomenon because the boiling can be expressed as a function of liquid position alone.

There are some conditions that tend to stabilize a system. In the upper model of figure IV-30, the liquid column contains gas bubbles. When oscillations involving strong interactions with the inertia of the liquid column are considered, the presence of the gas provides some compressibility in the liquid column tending to reduce the severity of the oscillations. While this mechanism would tend to reduce the severity of the initial surge, it could lead the system into the mode of oscillation related to a variation in inlet quality.

Perhaps the most widely used stabilizing influence in boiling systems is indicated in the lower model of figure IV-30. A restriction in the liquid region just before the boiling section will nearly always stabilize a system. It does this either by isolating the inertia of the liquid from the boiling process, or by making the amplitude of the two-phase oscillations small in terms of the total pressure loss through the system.

This approach is difficult to apply to a transient case because the depth of liquid penetration is changing with time making the restriction location a difficult problem. This approach also increases the pump work. As pointed out previously, flashing at the restriction can lead to a mode of oscillation related to the nucleation source.

Summary of Oscillations

The oscillation-source and nucleation-source modes were primarily a result of periodic variation in two basic parameters: flow rate and/or inlet quality. The strong influence of these parameters on pressure drop has been discussed previously. The density wave mode of oscillation is related to boiling primarily in the sense that it reflects the periodicity of the slug-mist flow model as it passes through a restriction. The initial surge mode could be considered as the seeking of a stable depth of liquid penetration that would satisfy the overall applied pressure drop. The variation in boiling rate during this seeking, acts as a forcing function. The significance or importance of each mode of oscillation is dependent on the system characteristics and operating conditions.

It has been the intent of this discussion to convey a physical explanation of the various modes observed in terms of understandable parameters. Analytically it is not this simple. Each mode involves a complex interaction of flow, heat transfer, fluid properties, and system geometric characteristics. Analytical models of systems to evaluate the various modes have met with only limited success because of difficulties in simulation of characteristics and weighting of the interactions.

CONCLUDING REMARKS

Studies related to reactor aftercooling are not discussed in this paper. References 6 and 7 (p. 133) are listed as representative of Lewis effort in this area. Analysis of the transient-flow characteristics in the laminar-turbulent transition region are being continued at Lewis (unpublished data obtained by R. W. Leko).

FLUID CONTROLS

Vernon D. Gebben

INTRODUCTION

The nuclear-rocket engine is composed of two separable but interacting systems. Energy is derived from a nuclear rocket that is controlled by neutron-absorbing material on control drums located in the reflector. Hydrogen flows through the reactor absorbing the heat generated and is expelled through a nozzle producing thrust. The system flow is regulated by the turbopump whose speed is controlled by the turbine-power-control valve. The most significant control parameters for operating the engine are the chamber temperature and the chamber pressure, which are indicative of specific impulse and thrust.

A simplified block diagram of a NERVA type control system is shown in figure IV-31. The programmer provides the reference signals for the reactor-power and the system-flow loops. The system controller contains comparators for measuring the difference between the reference signals from the programmer and the feedback signals, amplifiers for high sensitivity, and compensators for stabilizing the system. Actuation servos are used to position the turbine-power-control valve and the control drums. The chamber pressure P_c and the chamber temperature T_c are the controlled variables that are measured for use by the system controller. Neutron flux signals φ are available for reactor startup and for quick reactor power control.

In the present control system, the elements are controlled by electrical signals, and the actuation servos are electropneumatic servomechanisms. Another approach, under investigation, is to use an all-pneumatic control system; that is, to replace electronic circuits with pneumatic circuits and to use pneumatic control sensors. The pneumatic supply would be hydrogen gas - the working fluid of the engine. In the pneumatic circuits, fluid amplifiers are the counterpart for the transistors, line restrictors are the resistors, and volumes are the capacitors. Integrated circuits can be fabricated by using techniques analogous to the printed circuit used in electronics.

For the past 3 years, Lewis has been evaluating pneumatic components that could be used to improve reliability without affecting the performance of the system. This paper describes the operation of some of the fluid amplifiers that are being used in these developments and presents the status of this work.

FLUID AMPLIFIERS

The fluid amplifier (also called fluidic and flueric) was introduced 6 years ago by the Army's Harry Diamond Laboratories. Figure IV-32 shows the silhouette of passageways

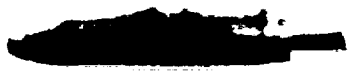

engraved in a block of material. The fluid that flows through the channels is gas, but liquid can be used. As illustrated, the high-pressure-supply flow is deflected to output channel 2. The deflection is caused by a low-pressure signal in control channel 1. Likewise, the supply would be deflected to the other output channel when the pressure in control channel 2 exceeds the pressure in control channel 1. The flow from the outputs would be directed to the control ports of another amplifier or, possibly, to a motor. This type of fluid amplifier can be built to operate as either a bistable or a proportional amplifier. In the bistable amplifier, the supply flow is switched from one output port to the other. In the proportional unit, the supply stream is divided into two outputs that are related to the differential control signal.

Figure IV-33 illustrates some Lewis design improvements (ref. 8, p. 133). In this unit, the control passageways inject the control flow in a direction along the supply stream rather than perpendicular, as shown in figure IV-32. This configuration prevents overdeflection of the supply stream and thereby produces good saturation characteristics.

The side vents provide another feature. Side vents A and the center vent C improve the performance by increasing the linearity and reducing the noise in the output. Side vents B are designed to isolate the amplifier from the load. Operation of side vents B is illustrated in figure IV-34 where the amplifier is driving a piston. As shown, the supply stream is deflected to the lower output passageway and directed into the lower chamber of the actuator. The piston moves upward. The fluid discharged from the upper chamber flows back into the amplifier. This return flow is diverted out the side vent. If, however, the amplifier did not have this special vent, the return flow would be directed into the sensitive interaction region and would interfere with proper operation of the amplifier. Tests have shown that side vents B are very effective buffers for isolating the amplifier from the load.

A photograph of one of our laboratory test models is shown in figure IV-35. This model is approximately 4 inches long and 2 inches wide. The channels are 1/16 inch deep. The width of the supply nozzle is 40 thousandths of an inch. This amplifier can be reduced to one-third of its present size by using photoengraving techniques. Photoengraving techniques have been used to build amplifiers with materials of plastic, glass, and metal.

One of the main features of this jet type of fluid amplifier compared with other fluid amplifiers is its high-frequency response. Fluid logic circuits have been demonstrated to operate with pulse rates of 1000 pulses per second.

Another important device in this field is the vortex amplifier (illustrated in fig. IV-36). It consists of two parts: a cylindrical chamber and a separate tube. The flow enters the chamber through radial inlets for supply flow and through tangential nozzles for control flow. The flow leaves the chamber through an orifice located at the center of chamber end-wall. The flow leaving the orifice is collected by the receiving tube located

a short distance away from the orifice. The flow that bypasses the tube is vented out. The pressure and flow collected in the tube are the output of the amplifier.

First, consider the case where the control flow is zero. The supply flow entering the chamber radially will flow directly to the exit orifice. The flow leaving the orifice will be a jet that flows into the receiving tube. This condition of zero control flow gives the maximum output; 95 percent pressure recovery and 95 percent flow recovery can be obtained. High recovery results because the distance between the exit orifice and the receiving tube is small.

When control flow is injected into the chamber, a vortex is generated. Consequently, the flow leaving the exit orifice is rotational flow that fans outward as the result of centrifugal forces. Because the flow from the orifice is conical in shape, the fluid will partially bypass the receiving tube. The amount of bypass depends on the strength of the vortex established by the control flow. With maximum control flow, all the fluid is vented. This operating condition gives the minimum pressure in the receiving tube, and an output pressure whose value is generally below the vent pressure.

In addition to the amplification characteristics resulting from the exit flow pattern, the vortex amplifier also throttles the flow leaving the exit orifice. (The exit flow equals the total of control and supply flows.) In some designs, the flow leaving the exit orifice is reduced by a factor of 8 when the control changes from zero to maximum flow rate because resistance to vortex flow is much higher than the resistance to radial flow. The combination of throttling and diversion of the fluid leaving the exit orifice provides a useful method for controlling power to a load.

Several other types of fluidic elements have been described in engineering literature. In general, each of these elements operates by a sensitive dynamic trait that controls the flow pattern of the supply (main) stream. Some elements operate by controlling the boundary layer, others use techniques that involve the control of fluid entrainment, turbulence, momentum, and vortex flow.

These elements appear to be well suited for application on the nuclear rocket. They can operate on hydrogen gas, have adequate frequency response characteristics, and can be built rugged for operating near the engine.

Actuation Servos

The actuation servos for the turbine-power-control valve and the control drums have been examined for possible improvements. The major components of the actuation servo are shown in figure IV-37. The servo consists of two assemblies: a control assembly for processing signals and an actuator assembly for power. The control assembly contains a comparator for measuring the difference between the input and feedback signals, ampli-

fiers for boosting signals, conditioners for stabilizing the system, and a speed limiter for preventing the actuator from slewing too fast. In the second assembly, the servovalve provides the pneumatic power to the motor, the motor manipulates the control drum (or turbine-power-control valve), and the position sensor provides the feedback signal. The control assembly, servovalve, and motor are three areas under investigation for improvements.

The new control assembly would use pneumatic circuits designed to tolerate the severe environment of extreme temperatures and radiation. This assembly will be mounted on the actuator assembly to form a single package instead of the two separate units required when electronics are used. The study phase of the contract showed that the servo operated with fluid-amplifier circuits will have the performance equivalent to the present electronic unit. The details on component sizes, amplifier requirements, and the pressure-flow requirements are available in references 9 and 10 (p. 133). Most of the components have been fabricated. Preliminary tests on portions of the compensation networks indicate that the required specifications can be obtained.

The servovalve shown in figure IV-38 operates without the use of moving mechanical parts. This experimental model used vortex amplifiers for controlling the fluid power. It was demonstrated that this type could be designed for use in the control drum actuation servos. Except for linearity and output stability, the performance of this unit is comparable to the flapper nozzle type presented used on the NERVA actuators. Summary of the performance characteristics are given in table IV-1. The final report (ref. 11, p. 133) presents design details, test results, and suggestions for improving the performance.

A second-generation flueric servovalve is presently under development. This new unit also uses vortex amplifiers for controlling the flow. Besides improving the linearity and noise characteristics, it will have higher power gain and will incorporate dynamic pressure feedback. This feedback provides virtual damping characteristics to the actuator and thereby stabilizes the system. This servovalve is being designed to operate in conjunction with the pneumatic control assembly.

The improved motor under development is the pneumatic nutator motor. This motor, shown in figure IV-39, was designed for manipulating the control drums of nuclear-rocket engines similar to NERVA. It is ideal for nuclear-rocket applications because it contains no high-speed sliding parts that require special lubricants.

The motor contains a pair of bevel gears with an unequal number of teeth. The input gear is attached to the housing by a gimbal ring and is driven by eight bellows. The gimbal ring allows the input gear to nutate (wobble) and prevents rotation. The output gear, which is attached directly to the output shaft, is allowed to rotate but not to nutate. By moving the point of force around the circumference of the input gear, the input gear will nutate and its teeth will mesh consecutively with each of the output gear teeth. The output gear has one less tooth than the input gear. Consequently, the output will be displaced

by one tooth for each cycle of the input gear. The bellows that manipulate the input gear are pressurized sequentially by a logic network of vortex amplifiers. A low-power pneumatic input signal controls the logic network, driving the motor in either direction.

The final report (ref. 12, p. 133) on this motor describes the operation and the test results. Some performance deficiencies were noted with the prototype motor. The maximum output speed of 10 degrees per second and the maximum output torque of 235 inch-pounds were too low. It should be pointed out, however, that low performance characteristics were caused by the fluid logic circuits and were not the fault of the mechanics of the motor. Improvements in the circuits are being developed. In general, the motor operated satisfactorily and demonstrated feasibility for use in control-drum systems.

CONCLUSIONS

These investigations for improving the NERVA control system revealed some difficulties in designing new fluid-amplifier circuits. For example, fluid elements were easy to demonstrate, but high performance circuits required extensive development. Exact impedance matching within the circuit is very important and generally requires a major effort to accomplish. Wave reflections can also create problems in high gain operational circuits used in control systems. Results from our work and from developments under other government programs, however, do indicate that fluidic control systems are feasible.

REFERENCES

1. Hendricks, R. C.; Simoneau, R. J.; and Friedman, R.: Heat-Transfer Characteristics of Cryogenic Hydrogen from 1000 to 2500 psia Flowing Upward in Uniformly Heated Straight Tubes. NASA TN D-2977, 1965.

2. Ellerbrock, Herman H.; Livingood, John N. B.; and Straight, David M.: Fluid-Flow and Heat-Transfer Problems in Nuclear Rockets. Nuclear Rocket Propulsion, NASA SP-20, 1962, pp. 27-56.

3. Hendricks, R. C.; Graham, R. W.; Hsu, Y. Y.; and Friedman, R.: Experimental Heat Transfer and Pressure Drop of Liquid Hydrogen Flowing Through a Heated Tube. NASA TN D-765, 1961.

4. Miller, John V.; and Taylor, Maynard F.: Improved Method of Prediction Surface Temperatures in Hydrogen-Cooled Nuclear Rocket Reactor at High Surface- to Bulk-Temperature Ratios. NASA TN D-2594, 1965.

5. Stenning, A. H.; and Veziroglu, T. N.: Boiling Flow Instability. Rep. No. 7 (NASA CR-64319), Miami Univ., Coral Gables (Fla.), May 1965.

6. Harry, David P., III: A Steady-State Analysis of the "Laminar-Instability" Problem Due to Heating Para-Hydrogen in Long, Slender Tubes. NASA TN D-2084, 1964.

7. Turney, G. E.; Smith, J. M.; and Juhasz, A. J.: Steady-State Investigation of Laminar-Flow Instability Problem Resulting From Relatively Large Increases in Temperature of Normal Hydrogen Gas Flowing in Small Diameter Heated Tube. NASA TN D-3347, 1966.

8. Griffin, W. S.: Bistable Fluid Jet Amplifier with Low Sensitivity to Receiver Reverse Flow. Proceedings of the Fluid Amplification Symposium, Harry Diamond Labs, Oct. 1965, vol. 3, pp. 17-35. (Available from DDC as AD-623457.)

9. Boothe, W. A.: Feasibility Study - Application of Fluid Amplifiers to Reactor Rod Control. Rep. No. 63-GL-134 (NASA CR-54005), General Electric Co., Nov. 25, 1963.

10. Cardon, M. H.: Replacement of Electronics with Fluid Interaction Devices. Rep. No. BRLD-2946 (NASA CR-54758), Bendix Corporation, Aug. 31, 1965.

11. Anon: Design, Fabrication and Test of a Fluid Interaction Servovalve. Rep. No. BRLD-2978(NASA CR-54463), Bendix Corporation, May 17, 1965.

12. Howland, G. R.: Pneumatic Nutator Actuator Motor. Rep. No. BPAD-863-16719R (NASA CR-54788), Bendix Corporation, Oct. 17, 1965.

TABLE IV-1. - SIGNIFICANT PERFORMANCE CHARACTERISTICS

Item	Specified	Measured
Supply pressure	5.16×10^5 N/m^2 g air (75 psig)	5.16×10^5 N/m^2 g air (75 psig)
Pressure recovery	3.1×10^5 N/m^2 g (min.) (45 psi)	3.1×10^5 N/m^2 (45 psi)
Rated no-load output flow	0.0113 kg/sec (0.025 lb/sec)	0.0131 kg/sec (0.029 lb/sec)
Flow recovery	0.55 min	0.44
Quiescent supply flow	0.0204 kg/sec (max.) (0.045 lb/sec)	0.030 kg/sec (0.067 lb/sec)
Input signal pressure	2.75×10^5 N/m^2 g (max.) (40 psig)	1.72×10^5 N/m^2 g (25 psig)
Input signal bias pressure	1.38×10^5 N/m^2 g (max.) (20 psig)	1.17×10^5 N/m^2 g (17 psig)
Input signal power	30 W (max.)	55 W
Differential input signal power change for output pressure change from -0.69×10^5 N/m^2 to 0.69×10^5 N/m^2 (-10 to 10 psi)	5 W (max.)	5 W
Linearity $\frac{\text{Gain maximum}}{\text{Gain minimum}}$	3	15
Output stability	0.034×10^5 N/m^2 (max.) (0.5 psi)	0.27×10^5 N/m^2 (4 psi)
Transient response	0.25 sec	0.10 sec

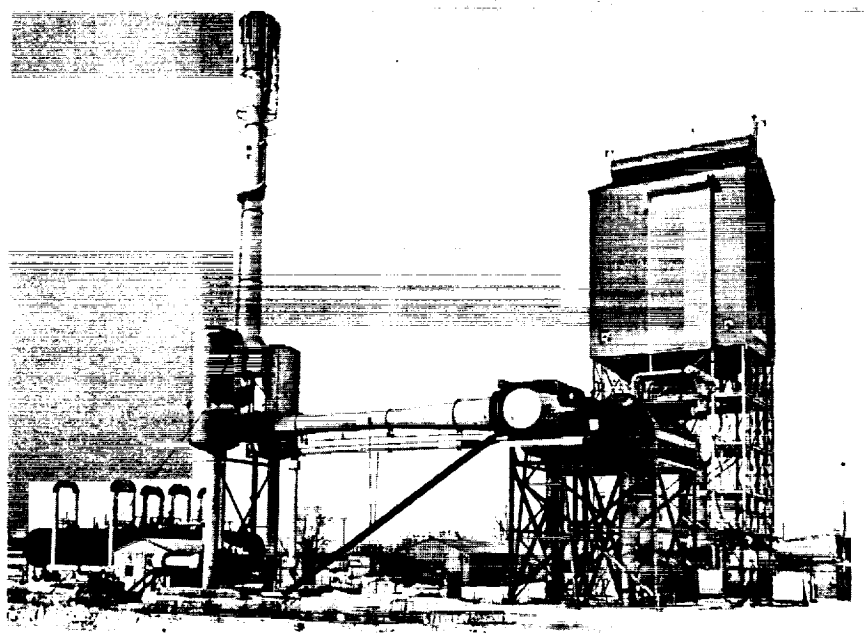

CS-39163

Figure IV-1. - Nuclear-rocket cold-flow test facility.

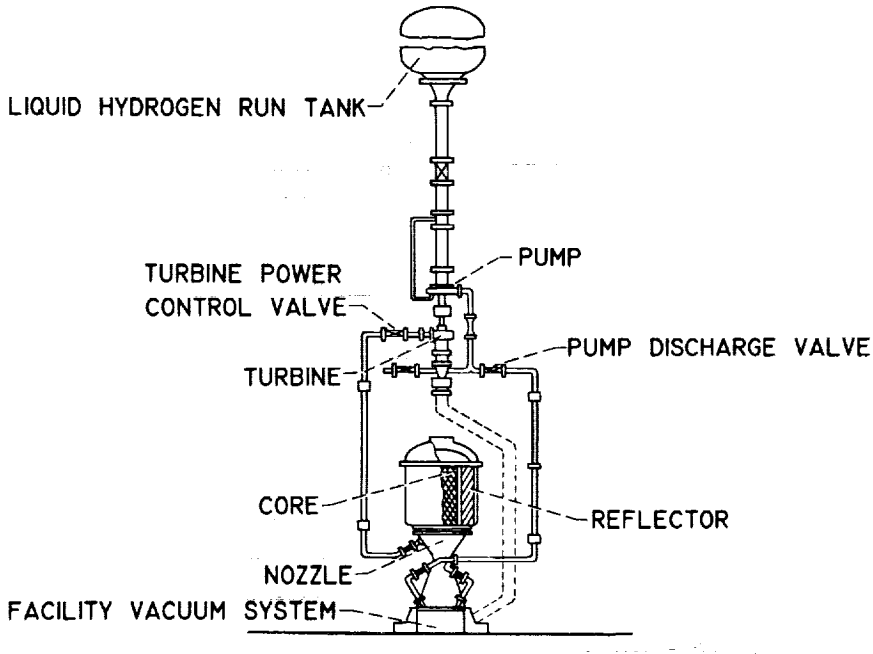

CS-39190

Figure IV-2. - Nuclear-rocket cold-flow-test hardware.

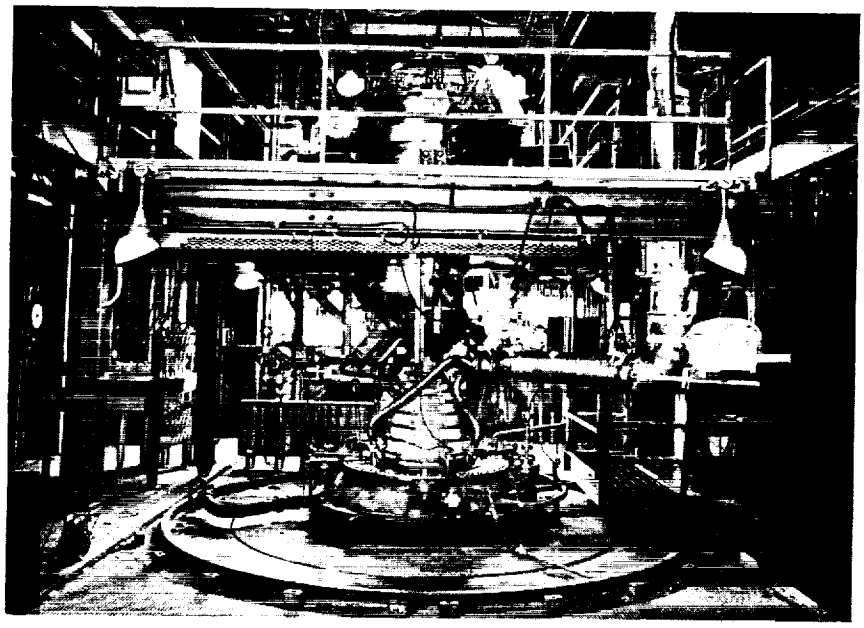

CS-39164

Figure IV-3. - Cold-flow startup test hardware.

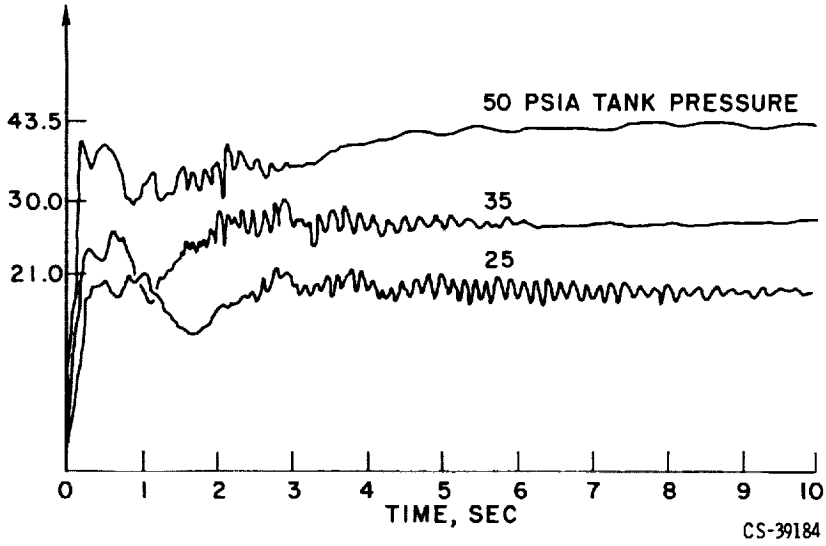

Figure IV-4. - Flow perturbations.

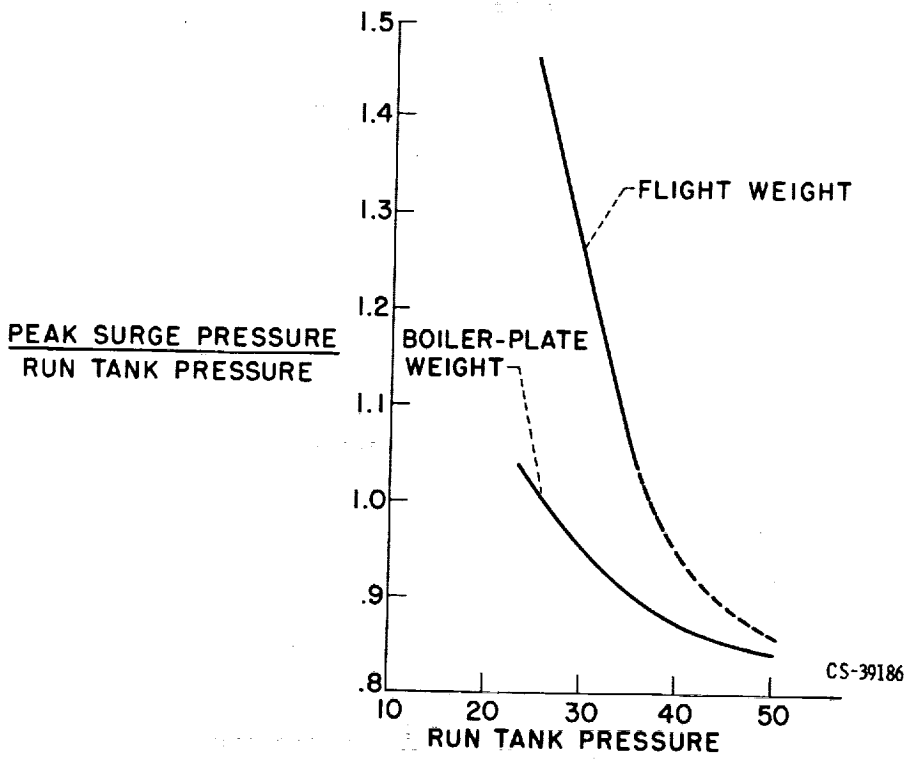

Figure IV-5. - Effects of tank pressure and flange weight on initial pressure surge.

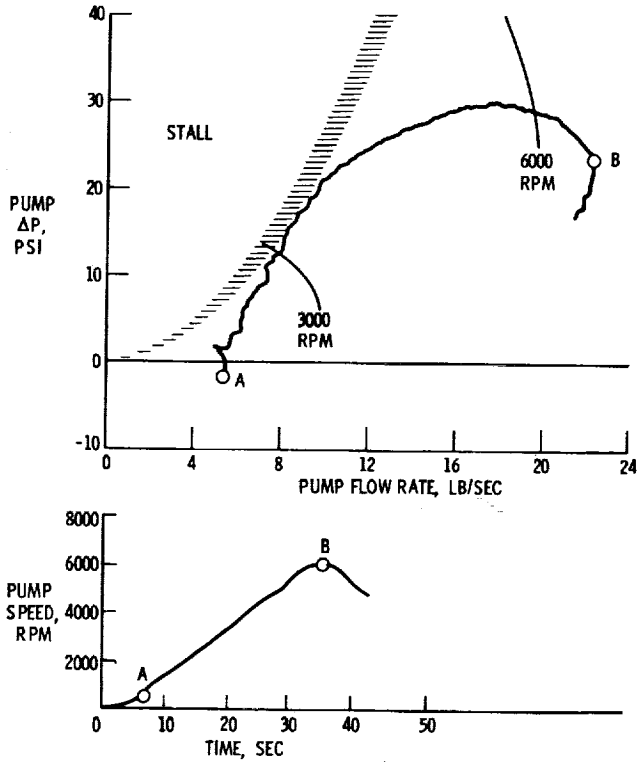

Figure IV-6. - Controlled bootstrap. Tank pressure, 35 pounds per square inch absolute.

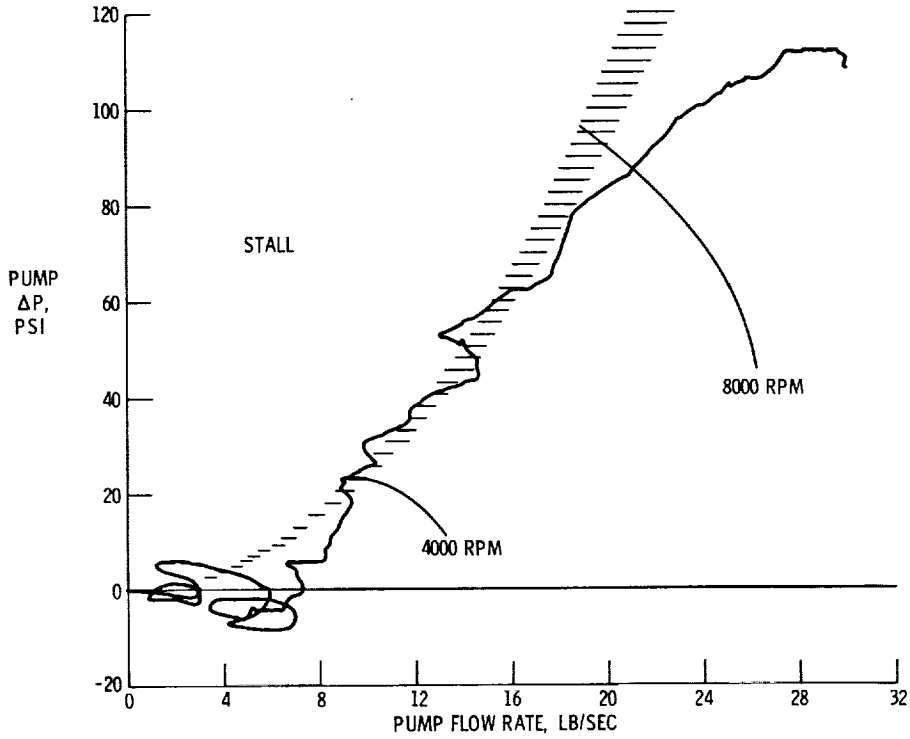

Figure IV-7. - Uncontrolled bootstrap. Tank pressure, 35 pounds per square inch absolute.

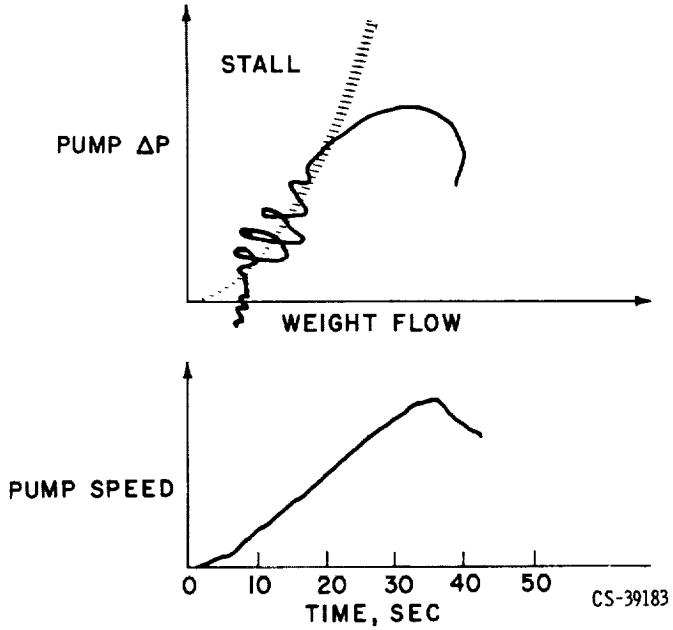

Figure IV-8. - Equipment operation problems.

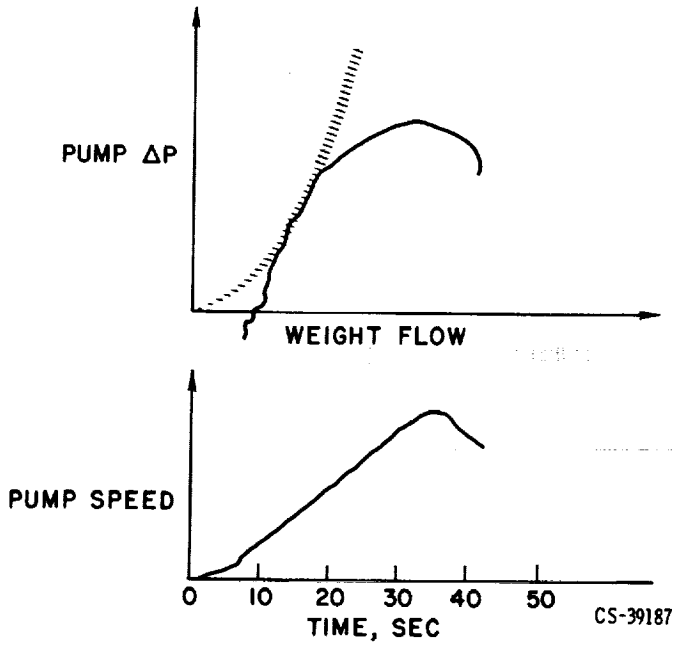

Figure IV-9. - Rerun with modified cold bleed line.

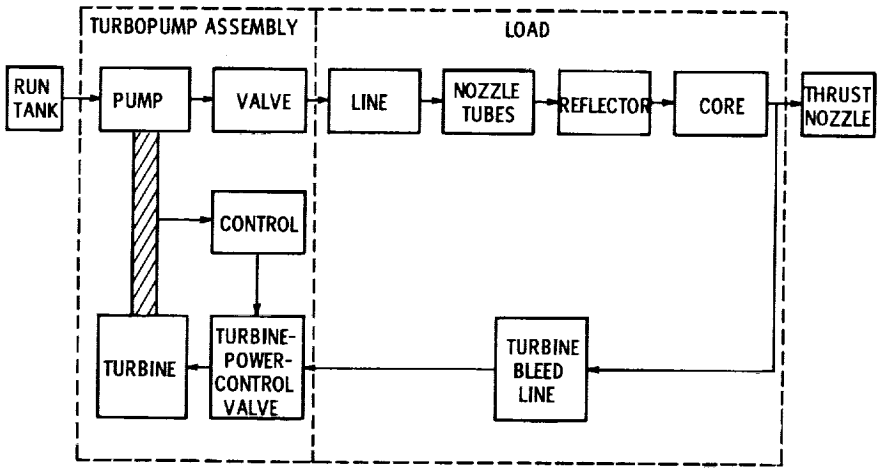

Figure IV-10. - System block diagram.

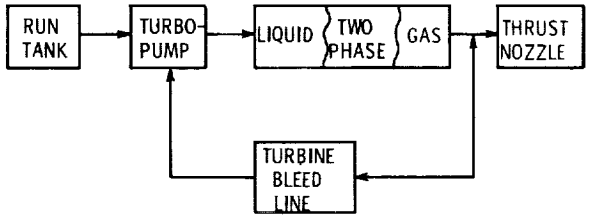

Figure IV-11. - Simplified model showing variation of fluid state throughout system.

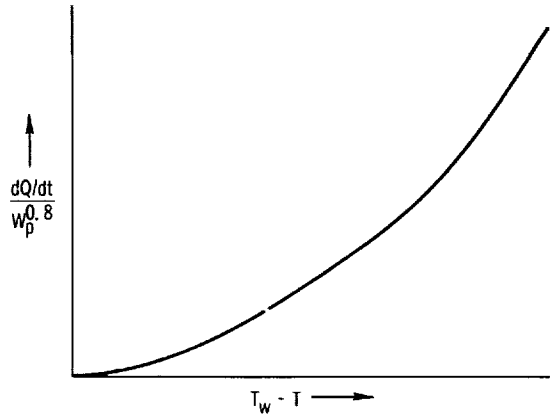

Figure IV-12. - Form of empirical heat-transfer correlation.

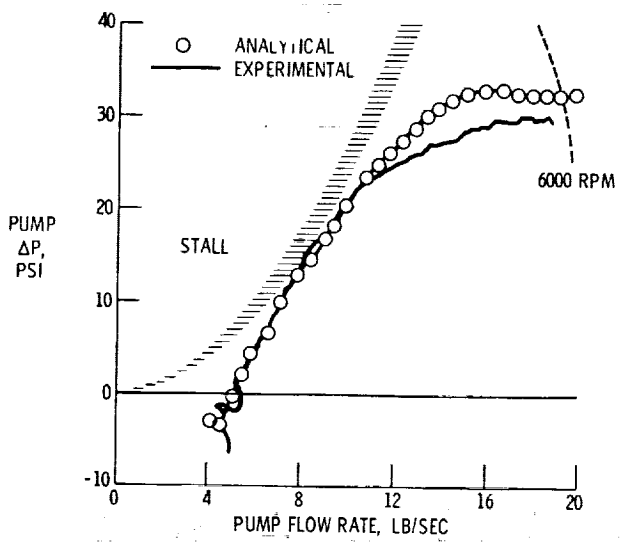

Figure IV-13. - Comparison of analytical and experimental controlled bootstrap data.

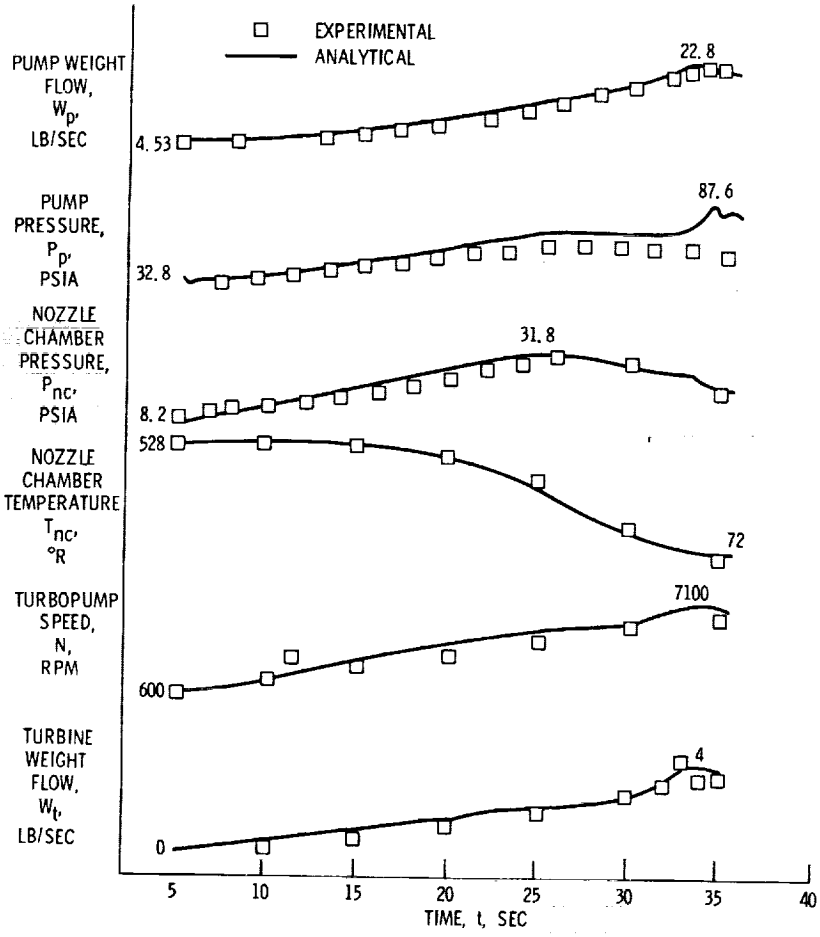

Figure IV-14. - Parameter-time comparison of analytical and experimental controlled bootstrap.

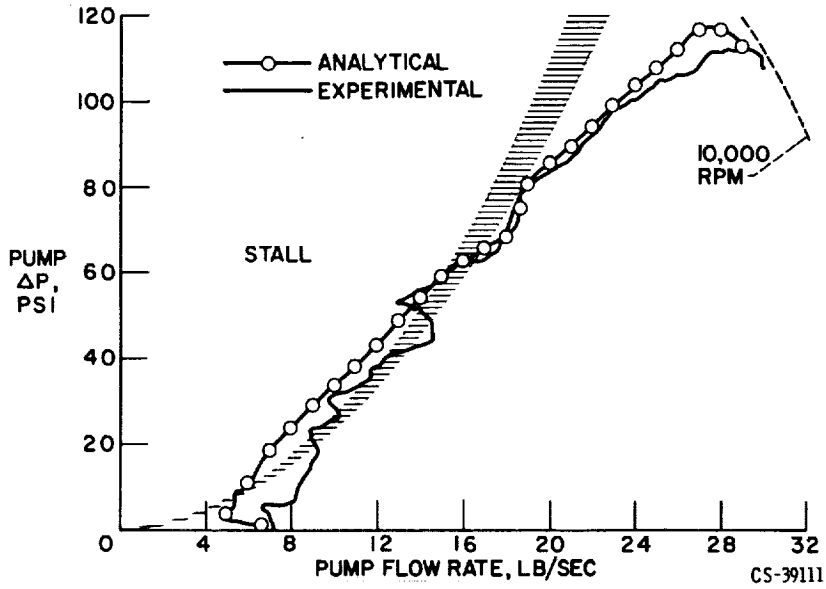

Figure IV-15. Comparison of analytical and experimental uncontrolled bootstrap data.

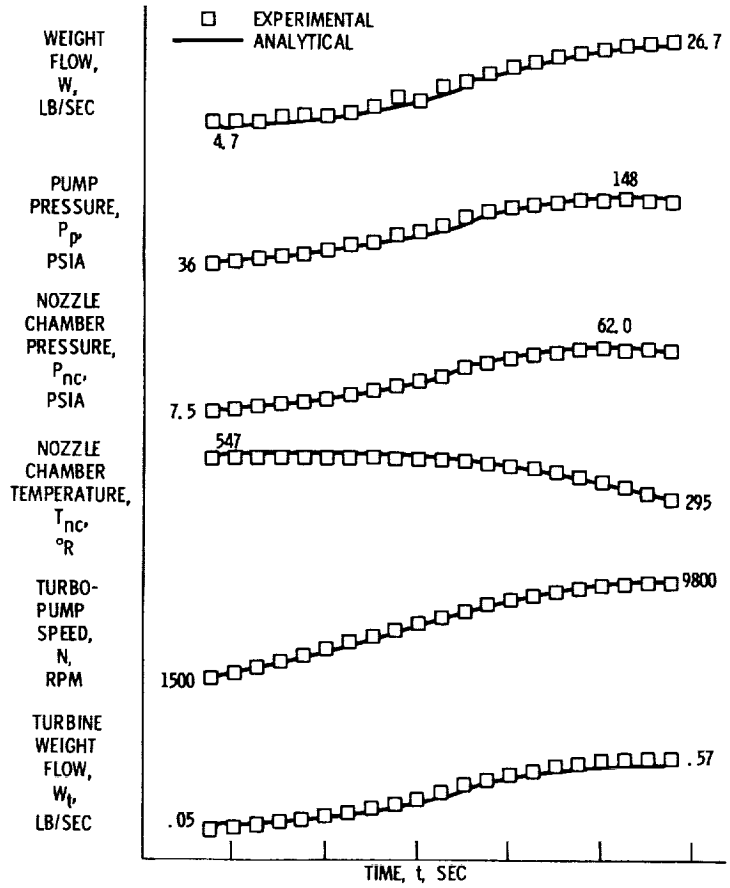

Figure IV-16. - Parameter-time comparison of analytical and experimental uncontrolled bootstrap.

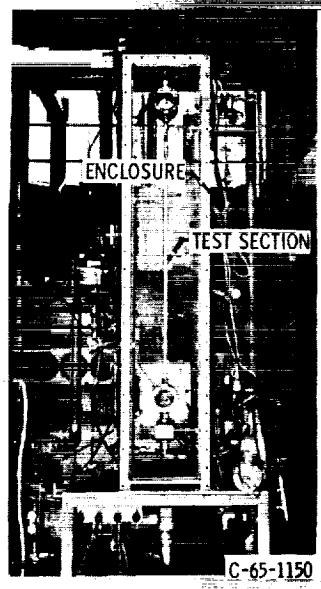

Figure IV-17. - Single thick walled tube.

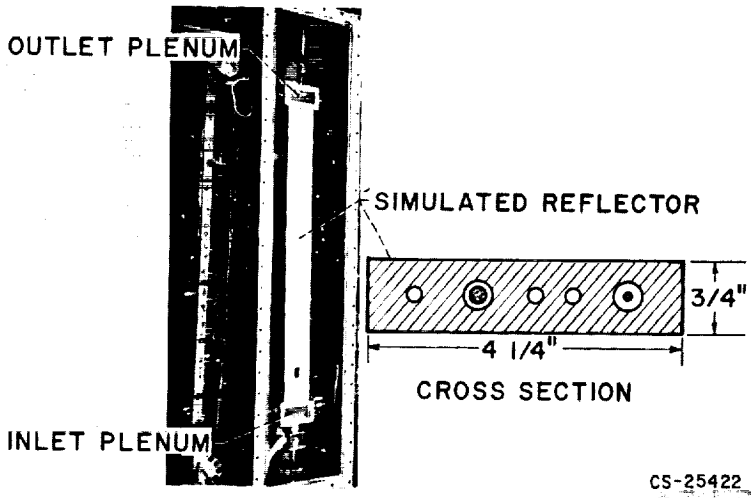

Figure IV-18. - Simulated reflector for flow maldistribution studies.

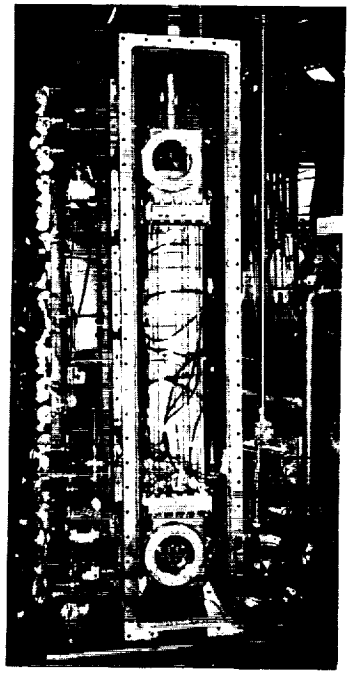

C-63961

Figure IV-19. - 1/24 reflector annulus.

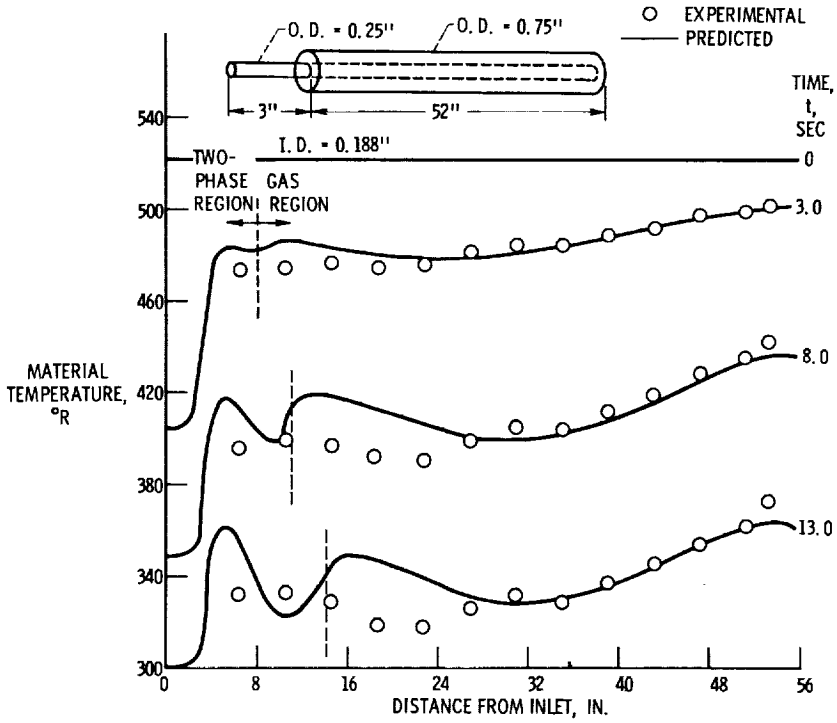

Figure IV-20. - Comparison of experimental and predicted wall temperatures as function of time during chilldown run.

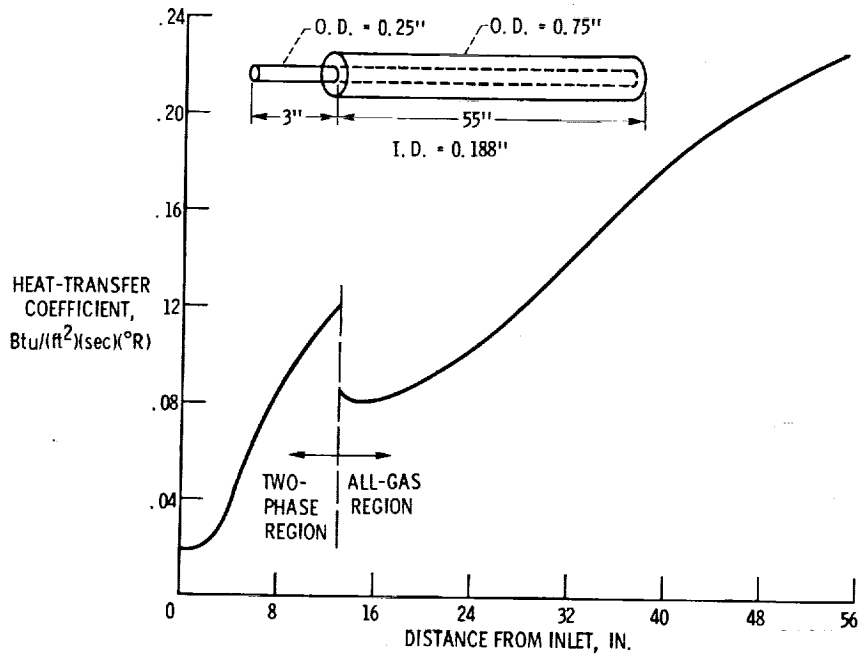

Figure IV-21. - Predicted heat-transfer coefficient as function of length. Chill-down run at 11.0 seconds; inlet pressure, 47.0 pounds per square inch absolute; 0.00644 pound per second; inlet enthalpy, 90.61 Btu per pound.

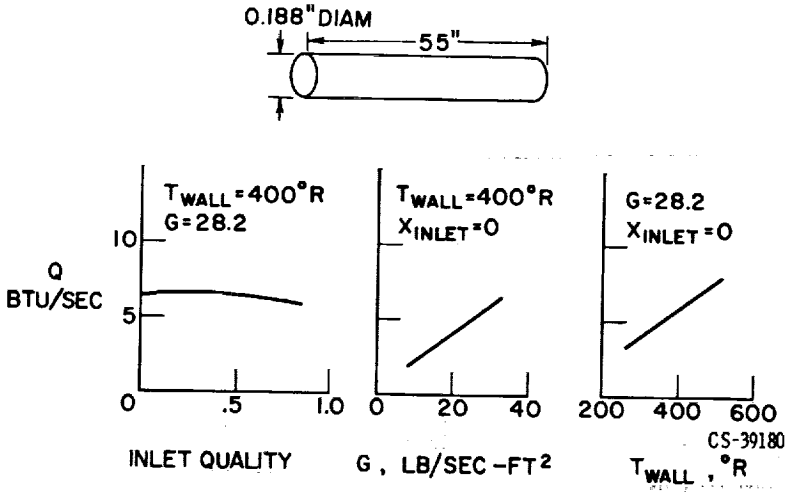

Figure IV-22. - Influence of quality, flow rate, and wall temperature on heat added to fluid.

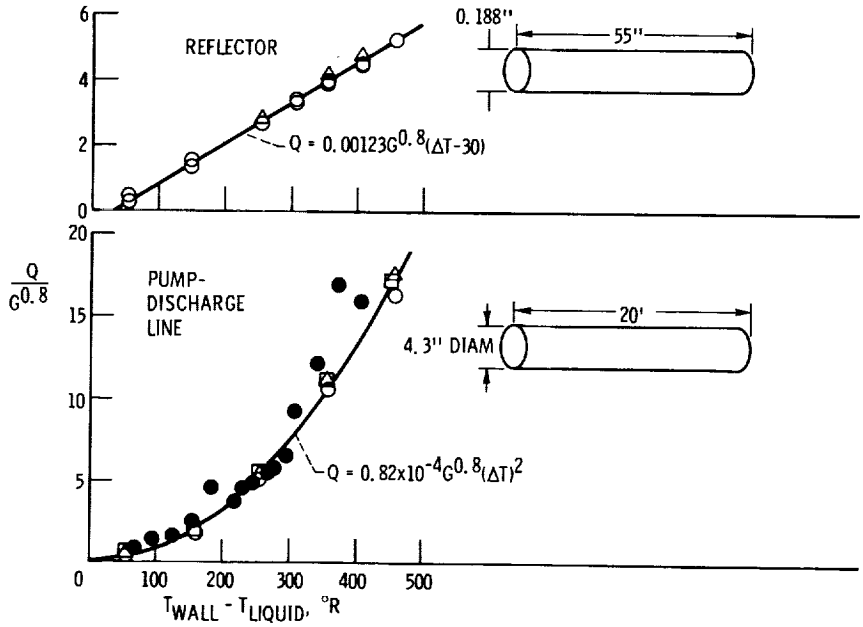

Figure IV-23. - Overall heat-transfer correlations.

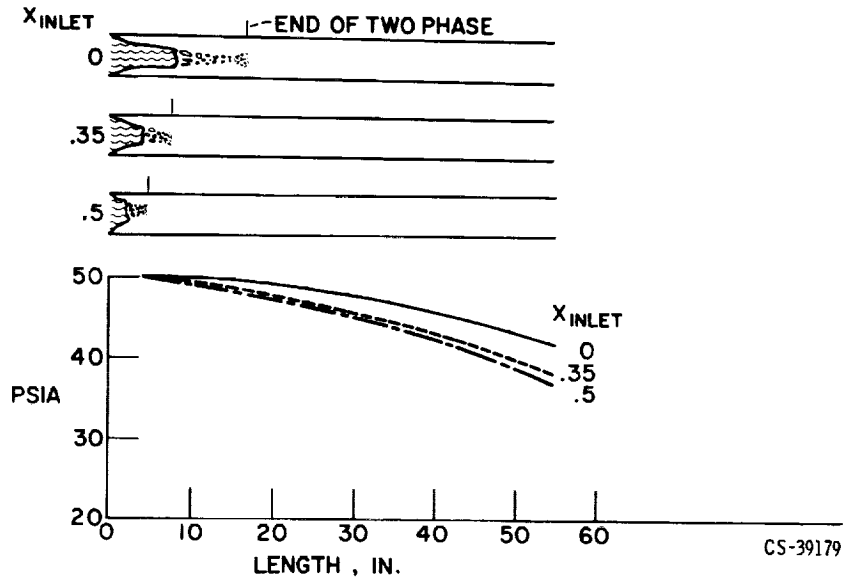

Figure IV-24. - Effect of inlet quality on pressure profile. Length, 55 inches; diameter, 0.188 inch; wall temperature, 300° R; inlet pressure, 50 pounds per square inch absolute; flow rate, 0.0052 pound per second.

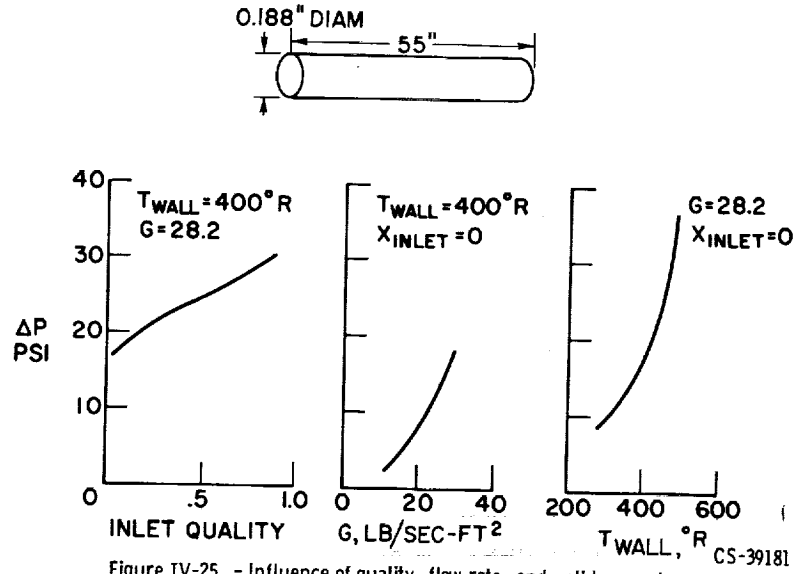

Figure IV-25. - Influence of quality, flow rate, and wall temperature on pressure drop.

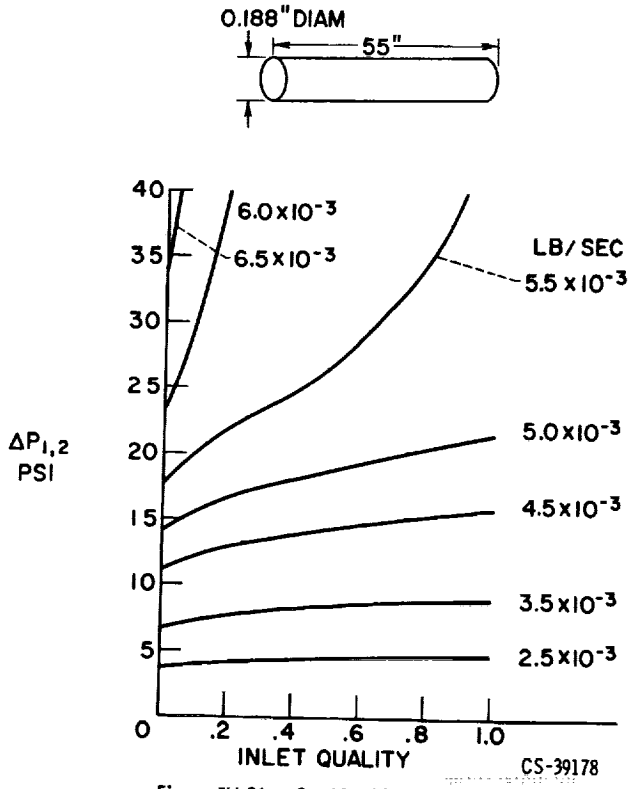

Figure IV-26. - Combined influence of inlet quality and flow rate. Wall temperature, 400° R.

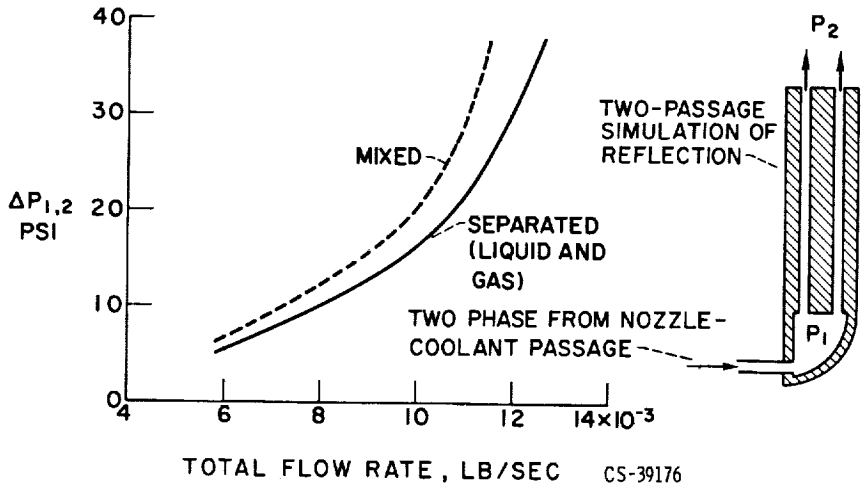

Figure IV-27. - Pressure drop as function of flow rate for separated and mixed inlet quality.

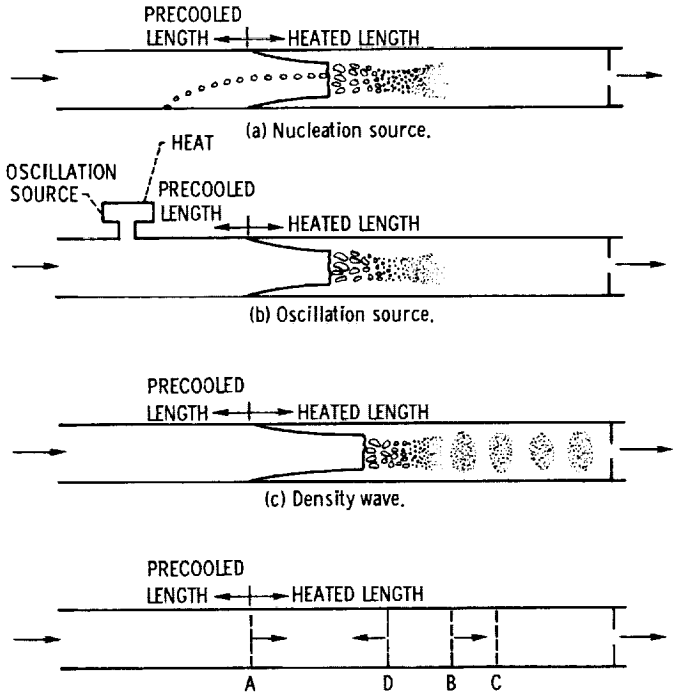

Figure IV-28. - Oscillation models.

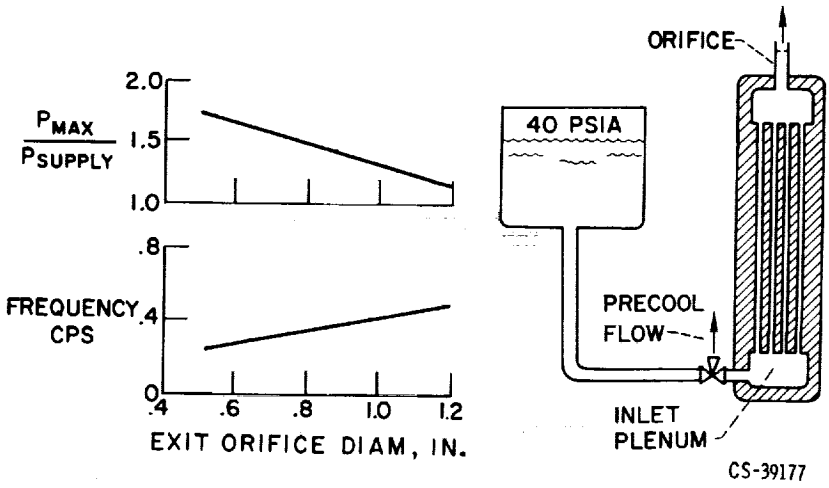

Figure IV-29. - 1/24th Reflector segment.

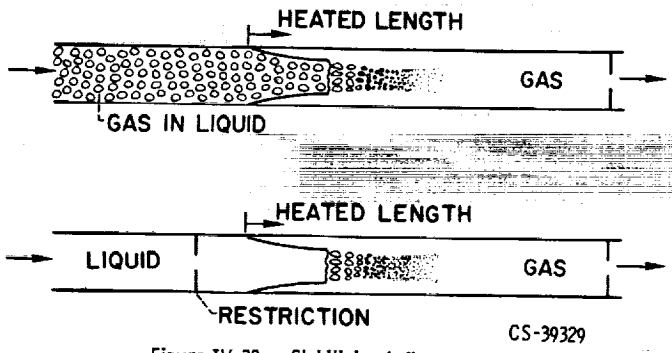

Figure IV-30. - Stabilizing influences.

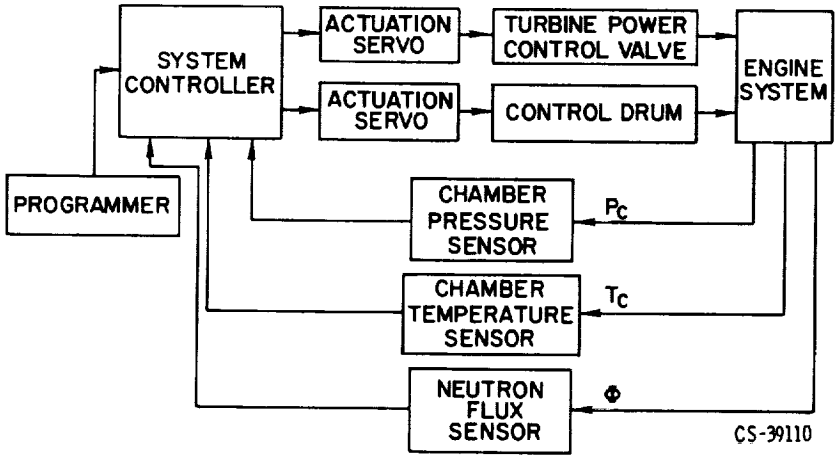

Figure IV-31. - Nuclear-rocket-engine control system.

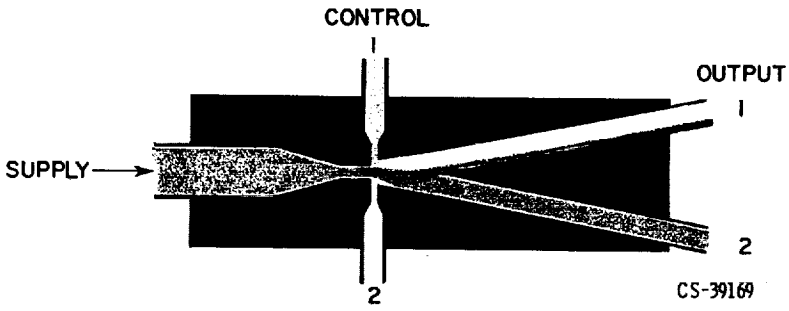

Figure IV-32. - Original fluid jet amplifier.

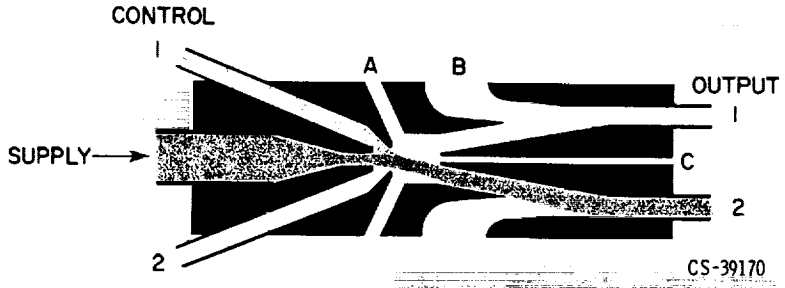

Figure IV-33. - Improved fluid jet amplifier.

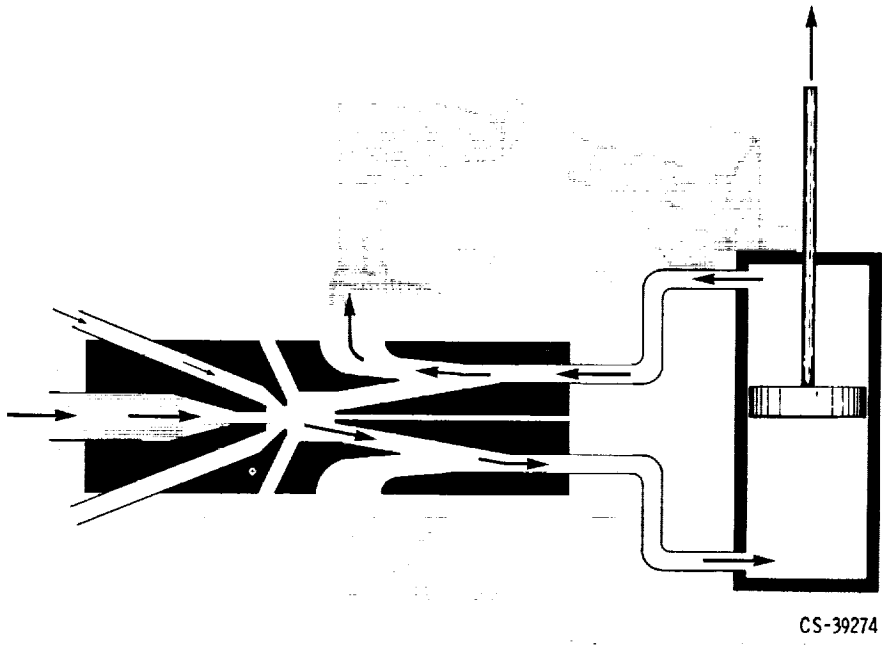

Figure IV-34. - Piston driven by fluid jet amplifier.

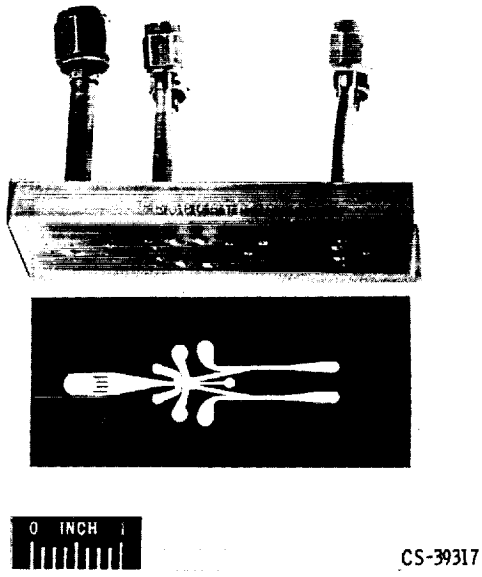

Figure IV-35. - Laboratory model of proportional amplifier.

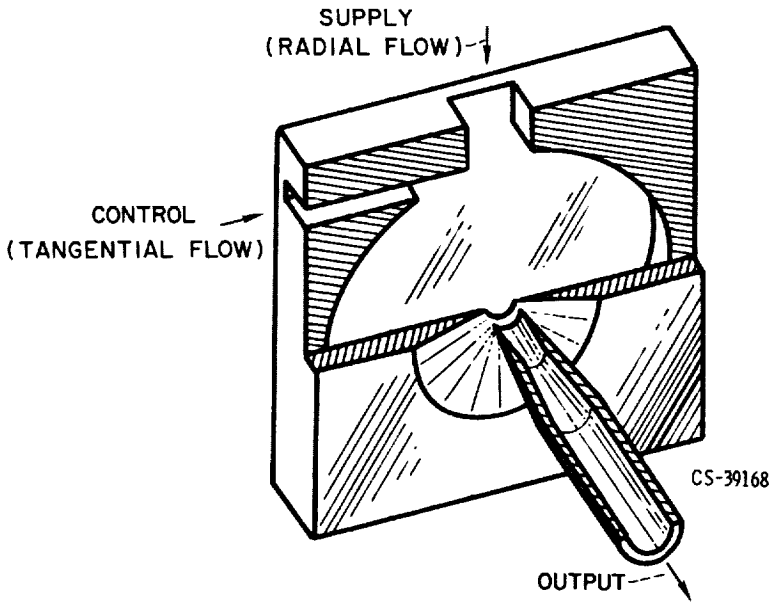

Figure IV-36. - Vortex amplifier.

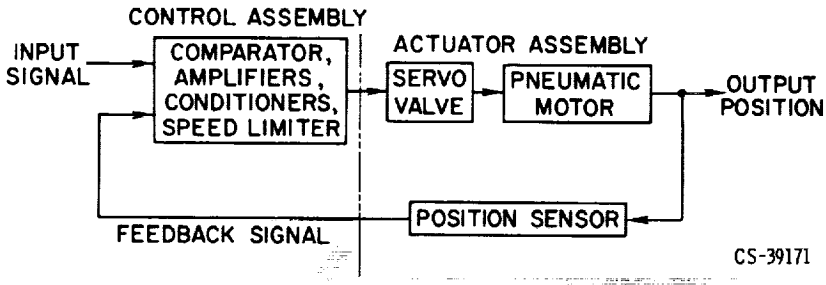

Figure IV-37. - Actuation servo for control drums and turbine-power-control valves.

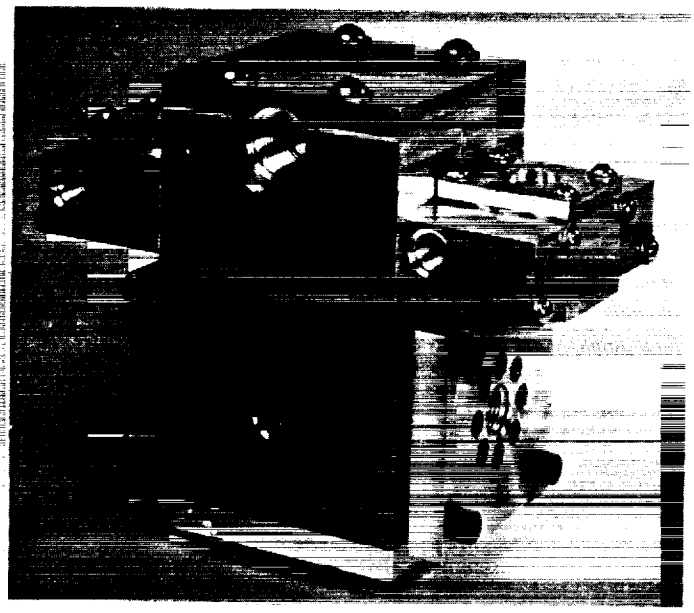

CS-39172

Figure IV-38. - Flueric servovalve.

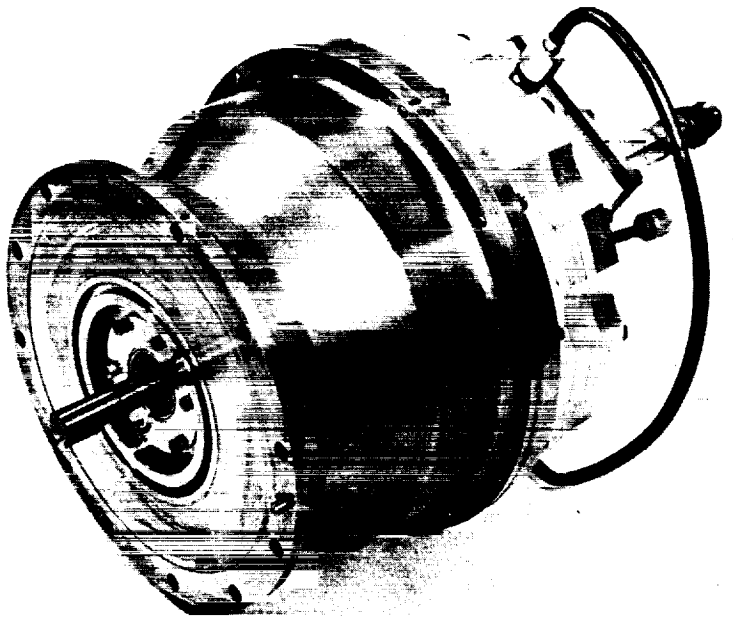

CS-39173

Figure IV-39. - Pneumatic nutator motor.